

Analysis of satellite-based Temperature Profiles using six-hourly Radiosonde Data at Neumayer Station, Antarctica

Master's thesis in Meteorology
by

Konstantin Krüger

November 2019



INSTITUT FÜR METEOROLOGIE UND KLIMAFORSCHUNG
KARLSRUHER INSTITUT FÜR TECHNOLOGIE (KIT)

Referent: Prof. Dr. Christoph Kottmeier
Co-referent: Prof. Dr. Jan Cermak



This document is licenced under the Creative Commons Attribution-ShareAlike 4.0 International Licence.

Abstract

Accurate satellite observations are crucial for Numerical Weather Prediction (NWP), particularly in the Antarctic, where the density of meteorological in-situ measurements is sparse. As part of the international field campaign “Year of Polar Prediction Special Observing Period Southern Hemisphere (YOPP-SOP-SH)” 339 radiosonde measurements were performed in six hour intervals at Neumayer Station (70°40'S, 8°16'W, 43 m a.s.l.). They provide a unique data set of temporally and vertically highly-resolved temperature profiles over the entire austral summer 18/19. The radiosonde temperature records are used to evaluate retrieved temperature profiles from the Atmospheric Infrared Sounder (AIRS) and the Infrared Atmospheric Sounding Interferometer (IASI) at a coastal site of Antarctica from the surface up to the middle stratosphere (30 km). AIRS and IASI profiles are matched within a circle of 50 km around Neumayer Station. The radiosonde observations are vertically interpolated to the pressure levels of the satellite products, while the collocated satellite profiles are temporally interpolated to the radiosonde record times.

For the entire YOPP-SOP-SH season, a slight negative bias of -0.14 K and a rmse of 0.97 K is found. Results show that the satellite data meets the accuracy demands of NWP for broad parts of the profile except for the tropopause region and the lowermost troposphere. The largest deviations between profiles occur at the surface level, at which the bias ranges between -8 to 8 K. Systematic biases are detected at certain levels of the profiles. The temperature minimum of the tropopause is typically overestimated by several degrees which is a consequence of the low vertical resolution of the satellite sounder. In the lower stratosphere weak positive and negative biases are continuously detected in the 50-250 hPa layer. A separate comparison of IASI and AIRS profiles indicates that these deviations are mainly caused by uncertainties of the AIRS profile. On the other hand the temperature in the lowermost troposphere is frequently underestimated,

since the diurnal temperature variations as part of the formation and regeneration of temperature inversions cannot be captured properly by the satellite products.

Our results demonstrate that errors due to horizontal and temporal mismatching are smaller than the effect of cloudiness. The impact of clouds on the accuracy of the satellite products is quantified by dividing the profiles into different categories of cloudiness according to the observed cloud cover and precipitation events at Neumayer Station. Clouds lead, especially in the troposphere, to larger errors of the satellite profiles since clouds predominantly occur in this atmospheric layer. The rmse increases by roughly 0.4 K from clear sky or slightly clouded to heavily clouded situations while the bias decreases by nearly 0.7 K. In the stratosphere errors do not show a significant relation to the observed cloud cover.

Generally, AIRS' and IASI's temperature products are able to capture surface-based temperature inversions. However, their attributes cannot be resolved accurately due to the limited vertical sounder resolution. For instance, temperature inversions are overestimated in frequency at any time of the day but their intensity is typically underestimated by the satellite products.

The results from this thesis contribute to an improved understanding of the accuracies and limitations of AIRS and IASI retrieved temperature profiles in the polar summer atmosphere.

Zusammenfassung

Präzise Satellitenmessungen sind besonders in der Antarktis von herausragender Bedeutung für die numerische Wettervorhersage, da dort aufgrund der klimatischen Extreme nur wenige Stationen meteorologische Informationen über den physikalischen Zustand der Atmosphäre bereitstellen. Im Rahmen der internationalen Messkampagne "Year of Polar Prediction Special Observing Period Southern Hemisphere (YOPP-SOP-SH)" wurden 339 Radiosondierungen alle sechs Stunden an der deutschen Polarforschungsstation Neumayer III (70°40'S, 8°16'W, 43 m ü. NN.) durchgeführt. Sie liefern einen einzigartigen Datensatz von zeitlich und vertikal hochaufgelösten Temperaturprofilen, der den gesamten südhemisphärischen Sommer 18/19 umfasst. Die Temperaturaufzeichnungen der Radiosonden werden verwendet, um von den Instrumenten „Atmospheric Infrared Sounder“ (AIRS) und „Infrared Atmospheric Sounding Interferometer“ (IASI) abgeleitete Temperaturprofile an einem küstennahen Standort der Antarktis von der Oberfläche bis hin zur mittleren Stratosphäre auszuwerten. Für die Evaluation werden alle AIRS- und IASI-Profile innerhalb eines Radius von 50 km um die Neumayer Station ausgewählt.

Für die gesamte YOPP-SOP-SH Saison ergeben sich ein schwach negativer Bias von -0,14 K, sowie ein Rmse von 0,97 K. In weiten Bereichen des Profils erfüllt die Genauigkeit der satellitengestützten Temperaturmessungen die Anforderungen numerischer Modelle. Die größten Abweichungen zwischen Radiosonden- und Satellitenprofilen treten an der Oberfläche auf, an welcher der Bias zeitweise Werte zwischen -8 und 8 K annehmen kann. Systematische Abweichungen treten in bestimmten Höhenniveaus der Profile auf. Das Temperaturminimum der Tropopause wird typischerweise um mehrere Grad überschätzt, was auf die geringe vertikale Auflösung der Satelliteninstrumente zurückzuführen ist. In der unteren Stratosphäre (50-250 hPa) treten kontinuierlich

schwache positive und negative Differenzen. Ein separater Abgleich der Temperaturprofile beider Instrumente deutet darauf hin, dass die systematischen Abweichungen in diesem Höhenbereich auf Ungenauigkeiten des AIRS Produkt zurückzuführen ist. Andererseits wird die Temperatur in der untersten Troposphäre häufig unterschätzt, da die tageszeitlichen Temperaturschwankungen im Zuge der Entstehung von Temperaturinversionen von den Satellitenprodukten nicht richtig erfasst werden können.

Darüber hinaus zeigt diese Studie, dass mögliche Fehler induziert durch zeitliche und räumliche Diskrepanzen von Radiosonden und Satellitendaten gegenüber dem Effekt von Bewölkung vernachlässigbar sind. Der Einfluss von Bewölkung auf die Genauigkeit der Satellitenprodukte wird untersucht, indem die Messreihe in verschiedene Bewölkungskategorien unterteilt wird. Für die Kategorisierung dienen die synoptisch visuellen Wetterbeobachtungen von Bedeckungsgrad und Niederschlagsereignissen, die an der Neumayer Station durchgeführt wurden. Wolken führen insbesondere in der Troposphäre zu erhöhten Fehlern der Satellitenprofile, da dort schließlich auch Wolken vorkommen. Im Vergleich zu wolkenlosen oder nur leicht bewölkten Profilen zeigen stark bewölkte Profile einen um etwa 0.4 K erhöhten der Rmse, während der Bias um 0.7 K fällt. In der Stratosphäre dagegen führt ein erhöhter Bewölkungsgrad nicht zu höheren Abweichungen.

Generell sind die abgeleiteten Temperaturprodukte von AIRS und IASI in der Lage Bodeninversionen zu erfassen. Aufgrund ihrer geringen vertikalen Ausdehnung, können spezifische Eigenschaften der Inversionen von den Satellitenprodukten jedoch nicht zutreffend wiedergegeben werden. So wird das Auftreten von Temperaturinversionen zu jeder Tageszeit überschätzt, wobei deren Intensität überwiegend unterschätzt wird.

Die Ergebnisse dieser Masterarbeit tragen zu einem verbesserten Verständnis der Genauigkeit und Limitierung von AIRS- und IASI- basierten Temperaturprodukten im polaren Sommer an einem küstennahen Standort der Antarktis bei.

Contents

1. Introduction	1
1.1 Motivation and objective	1
1.2 Previous studies of AIRS and IASI in the Antarctic	5
1.3 Theory of satellite measurements	7
2. Satellite and radiosonde data	13
2.1 Satellite observations	13
2.1.1 The infrared sounder IASI on Metop.....	14
2.1.2 The infrared sounder AIRS on AQUA.....	16
2.1.3 Data access and availability	17
2.2 Radiosonde observations.....	19
2.2.1 Vaisala RS41-SGP radiosondes.	19
2.2.2 Data access and availability	21
3. Methodology of data processing	23
3.1 Data post-processing scheme.....	23
3.1.1 Quality check.....	24
3.1.2 Collocation criteria and surface adjustments	25
3.1.3 Interpolation of the radiosonde and satellite data	27
3.2 Statistical metrics	31
4 Analysis of the temperature profiles	33
4.1 General comparison	33
4.2 Comparison of AIRS and IASI.....	42
4.3 Temporal mismatch.....	43
4.4 Horizontal mismatch.....	45
4.5 Impact of cloud cover	46
4.6 Surface-based temperature inversions.....	48
5 Discussion	51
6 Summary and outlook	59

List of abbreviations

AIRS	Atmospheric Infrared Sounder
AMSU	Advanced Microwave Sounding Unit
AVHRR	Advanced Very High Resolution Radiometer
AWI	Alfred-Wegener-Institute Helmholtz Centre for Polar and Marine Research
DEM	Digital Elevation Model
ECMWF	European Centre for Medium-range Weather Forecast
EOP	Earth Observation Portal
EUMETSAT	European Organisation for the Exploitation of Meteorological Satellites
FG	First Guess
FTS	Fourier Transform Spectrometer
GES DISC	Goddard Earth Sciences Data and Information Services Center
GFS	Global Forecast System
GTS	Global Telecommunication System
HSB	Humidity Sounder for Brazil
IASI	Infrared Atmospheric Sounding Interferometer
IFOV	Instantaneous Field of View
IPCC	Intergovernmental Panel on Climate Change
IR	Infrared
MetOp	Meteorological Operational satellite programme
MHS	Microwave Humidity Sounder
MW	Microwave
NASA	National Aeronautics and Space Administration

NCEP	National Centers for Environmental Prediction
NWP	Numerical Weather Prediction
PCC	Pearson-Correlation-Coefficient
RMSE	Root-Mean-Square-Error
RTE	Radiative-Transfer-Equation
SBTI	Surface-based Temperature Inversion
SCAR	Scientific Committee of Antarctic Research
SMD	Science Mission Directorate
SOP-SH	Special Observing Period Southern Hemisphere
WMO	World Meteorological Organisation
WWRP	World Weather Research Project
YOPP	Year of Polar Prediction

List of figures

Figure 1.1	The German research station Neumayer III on the Ekström ice-shelf	4
Figure 1.2	Bathymetric chart of the Antarctic and Sentinel-1 image of the Ekström ice-shelf	5
Figure 2.1	The instrument IASI on Metop	15
Figure 2.2	Availability of AIRS and IASI data during YOPP-SOP-SH	18
Figure 2.3	Radiosonde ascent tracks at Neumayer Station during the YOPP-SOP-SH	22
Figure 3.1	Overview of the three steps of the data processing	23
Figure 3.2	Birds-eye view for the northern edge of the Ekström ice-shelf	26
Figure 3.3	Comparison of the three methods of temporal interpolation	29
Figure 3.4	Exemplary profiles of temperature and rmse on the 10 th of January, 2019	31
Figure 4.1	Time-pressure evolution of temperatures recorded by the radiosondes at original vertical sampling resolution	34
Figure 4.2	Time-pressure evolution of temperatures based on AIRS and IASI profiles at the pressure grid of the level 2 products	34
Figure 4.3	Time-pressure evolution of temperatures recorded by the radiosondes and interpolated at the pressure grid of the level 2 products	35
Figure 4.4	Time-pressure evolution of temporally interpolated IASI/AIRS temperature profiles at the pressure grid of the level 2 products ...	35
Figure 4.5	Time-pressure evolution of temperature bias at the pressure grid of the level 2 products and at radiosonde measurement times	37
Figure 4.6	Time-pressure evolution of temperature rmse at the pressure grid of the level 2 products and at radiosonde measurement times	37

Figure 4.7	Profiles of temperature, bias and rmse averaged for the entire YOPP-SOP-SH	38
Figure 4.8	Time series of temperature bias and rmse for different vertical layers	39
Figure 4.9	Scatter plot of radiosonde and satellite temperatures coloured by their altitude and the corresponding vertical profile of the PCC	40
Figure 4.10	Scatter plot of radiosonde and satellite temperatures for the four main synoptic times and the corresponding vertical profile of the PCC	41
Figure 4.11	Separate analysis of IASI and AIRS temperature product concerning full profile, bias and rmse averaged for observations at 00 UTC	42
Figure 4.12	Temporal mismatch	44
Figure 4.13	Scatter plot of rmse and temporal mismatch and profile of rmse averaged for different bins of temporal mismatch	44
Figure 4.14	Scatter plot of rmse and horizontal mismatch and profile of rmse averaged for different bins of horizontal mismatch	45
Figure 4.15	Temperature bias and its standard deviation averaged for the categories of cloudiness and for different altitude levels	47
Figure 4.16	Temperature bias and its standard deviation averaged for the categories of cloudiness and for different altitude levels	47
Figure 4.17	Temperature profiles of the lowermost troposphere	49

List of tables

Table 2.1	Characteristics of AIRS and IASI	14
Table 2.2	Sensors and uncertainties of Vaisala's radiosonde RS41-SGP	20
Table 2.3	Radiosonde ascent statistics	21
Table 3.1	Key disparities of radiosonde and satellite measurements	24
Table 4.1	Average of rmse (bias) for the synoptic standard times and the entire period	40
Table 4.2	Categories of cloudiness: Classification and number of occurrence	46
Table 4.3	Rmse (bias) averaged for the categories of cloudiness and for the different atmospheric layers	46
Table 4.4	Attributes of SBTIs detected by the radiosondes	48
Table 4.5	Attributes of SBTIs detected by the satellite products	48

1. Introduction

1.1 Motivation and objective

In this thesis, meteorological data from radiosondes and three satellite instruments are assimilated for Neumayer Station location. These data sets offer the unique possibility to evaluate the reliability of satellite-based measurements directly at a polar location over a three months period under different weather conditions. Core to the study are two time series of temperature. The first is purely based on the six-hourly radiosonde observations and the second consists of satellite data from three hyperspectral infrared sounders: AIRS, IASI-A and IASI-B. Profiles extend from the surface up to the middle stratosphere at about 30 kilometres. Hence, the satellite time series can be evaluated in terms of a daily cycle, different weather situations and for specific layers of the atmosphere. Comparison of the time series is performed to identify and quantify the main sources of deviations between the satellite and the radiosonde temperatures during the Antarctic summer season. This work aims to clarify to what extent combined satellite products can be used to compensate for the lack of in-situ observations at Neumayer Station.

The Antarctic is strongly involved in climate change and takes a fundamental role in the global climate system through strong interactions between the atmosphere, cryosphere and hydrosphere such as changes of ice sheets and sea-ice extent, deep water formation and ozone budget (IPCC, 2013 and SCAR, 2009). According to the atmospheric temperature, climate change appears to have spatially and temporally varying impacts on the Antarctic (Johanson and Fu, 2007). The Southern Ocean and the Antarctic Peninsula experience a steady warming, but trends of increasing surface air temperatures cannot be identified for other parts of Antarctica (SCAR, 2009; König-Langlo and Loose, 2007). This variability of temperature trends is determined by changes in atmospheric circulation patterns, ozone budget, growing concentration of greenhouse gases

and natural variability (IPCC, 2013), however impact of climate change on the Antarctic is still subject of current research.

Weather and climate predictions depend not only on the quality of numerical models but also on reliable and accurate information about the current physical state of the atmosphere, which is captured by various meteorological observation platforms. The majority of atmospheric measurements for numerical weather prediction (NWP) are provided by geostationary and polar-orbiting satellites which are able to provide meteorological data for the entire globe (ECMWF, 2019). In principle, forecast quality improves with an increased number and accuracy of meteorological measurements. Radiosondes contribute substantially to forecast quality, as they record meteorological variables at high vertical resolution and with high precision. Limitations of the radiosondes are their spatial bias, due to the need for manned ground stations which do not exist in the oceans or vast regions of Antarctica. Although the Antarctic is an essential part of the climate system, the predictability of its weather and climate is still poor, mainly due to a lack of meteorological in-situ observations (SCAR, 2009). Antarctic's environmental conditions make collecting meteorological observations extremely challenging. Coastal sites and sites located at the Southern Ocean are frequently passed by severe storms making them one of the windiest regions of Earth. Antarctica's elevated interior on the other hand, is almost completely isolated from maritime influence, making it the coldest and driest place in the world. The density of permanently manned research stations where in-situ measurements are routinely taken is sparse in Antarctica due to its climatological extremes and peripheral geographical location. As a result, stations are predominantly located on coastal sites. Thus, observations made by polar-orbiting satellites become the most important source of meteorological information for numerical models at high latitudes as they provide meteorological data several times per day for a particular site (ECMWF, 2019). Advantageous for their high horizontal and temporal coverage, satellite observations are however limited in precision as they receive radiances only, which have to be converted by mathematical iterations. It is necessary, therefore, to evaluate satellite retrieved products with higher-quality in-situ data especially in regions such as the Antarctic.

Temperature inversions in particular are a formative feature of the polar atmosphere even though they occur in other parts of the world. Polar temperature inversions exhibit a concise diurnal and seasonal cycle and can change rapidly in terms of intensity, height and frequency of occurrence depending on the underlying synoptic situation. Antarctic temperature inversions are stronger and more persistent in winter than in summer season (Zhang et al., 2011). Studies

have shown that sea-ice formation or regeneration is directly related to snow cover (Kottmeier et al., 2003) as well as to the presence of surface-based temperature inversions (SBTI) (Mernhild and Liston, 2010). Moreover, SBTIs maintain vertical fluxes of energy and moisture from lower-tropospheric levels and thus exert influence on cloud formation and boundary layer chemistry (Andreas, 1980, Davis et. al., 2001).

Heterogeneous surface properties (e.g. ice, sea-ice, snow) and weather extremes (storms, cloudiness, temperatures) in the Antarctic can lead to substantial differences between satellite retrievals and the true physical state of the atmosphere (Boylan et. al 2016). As the meteorological conditions in the Antarctic differ strongly depending on the investigated region, the quality of satellite-based products is expected to differ for different locations. Hence, there is a need for evaluation of satellite products for particular sites in the Antarctic. In order to evaluate the benefit of satellite observation at Neumayer Station, this study deals with the comparison of radiosonde and satellite-based temperature time series during the polar summer season.

Field campaign YOPP-SOP-SH

As part of the “Year of Polar Prediction” (YOPP) campaign, an effort by the World Meteorological Organization’s (WMO) World Weather Research Project (WWRP), a special observing period (SOP-SH) was conducted in the Antarctic polar summer between November, 15th 2018 and February, 16th 2019. Cryospheric and atmospheric observations were carried out at Neumayer Station. During this period, in-situ radiosonde measurements were increased from once per day to four times per day at the main meteorological synoptic times 00 UTC, 06 UTC, 12 UTC and 18 UTC. The radiosondes measured important meteorological quantities such as temperature, pressure, humidity and wind with highest accuracy from the surface up to an elevation of more than 30 kilometres. The data set provides a time series of atmospheric profiles at unprecedented observation frequency of six hours recorded with high measuring precision for the entire 2018/19 polar summer season.

Neumayer station location



Figure 1.1: The German research station Neumayer III on the Ekström ice-shelf.

The German research station Neumayer III ($70^{\circ}40'S$, $8^{\circ}16'W$, 43 metres a.s.l.) operated by the Alfred-Wegener-Institute Helmholtz Centre for Polar and Marine Research (AWI) is located on the Ekström ice-shelf in the Atlantic sector of the Antarctic coast (figure 1.2). Neumayer Station is situated about 20 kilometres south of the shelf ice edge, so it experiences a maritime climate determined by the Southern Ocean. The climate is characterized by regularly passing cyclones that alternate with anticyclones. Heavy winds and precipitation during cyclonic events and clear sky or stratocumulus cloud cover and weak katabatic winds during anticyclones. The seasonal variation of sea-ice distribution is responsible for a strong seasonality of the climate at Neumayer Station. In summer the 2-meter air temperature occasionally rises to around 0 degrees Celsius, when the incoming solar radiation reaches its maximum. During the winter period, extreme temperatures of below minus 40 degrees Celsius are regularly recorded. SBTI can be observed throughout the year, although they are most pronounced in winter season (König-Langlo and Loose, 2007). In general, temperature inversion development and dissolution depend on the diurnal position of the sun and on the synoptic situation. Temperature inversions can form in vast parts of the world. At night the energy budget at surface is dominated by longwave irradiation, so temperatures in the lowermost levels of the atmosphere can decrease rapidly. This effect becomes most effective in windless and clear sky conditions and over snow, since snow is approximately a perfect emitter. Hence, over the course of the night strong surface inversions can form. The high sun's position during the day leads to a positive radiation balance which leads to heating of the lowermost tropospheric levels and thus a dissolution of the inversions around noon. This is a typical diurnal cycle of formation and degradation of inversions and can be

observed worldwide if the synoptic conditions are favourable. At Neumayer Station the diurnal variation of the sun's position is weak during austral summer but sufficient to drive this daily cycle of inversions. As formation of SBTI are bound to calm weather conditions, during storm events or in heavily clouded scenes no significant nocturnal inversions can form.

As Neumayer is located on an ice-shelf the surrounding relief is flat. The nearest elevation, known as Halvfarryggen, with an elevation of 400 metres, is located about 40 kilometres southeast of the station. Since the Ekström ice-shelf extends to the west of the station no hill of major importance is found in the proximate surrounding of Neumayer III.

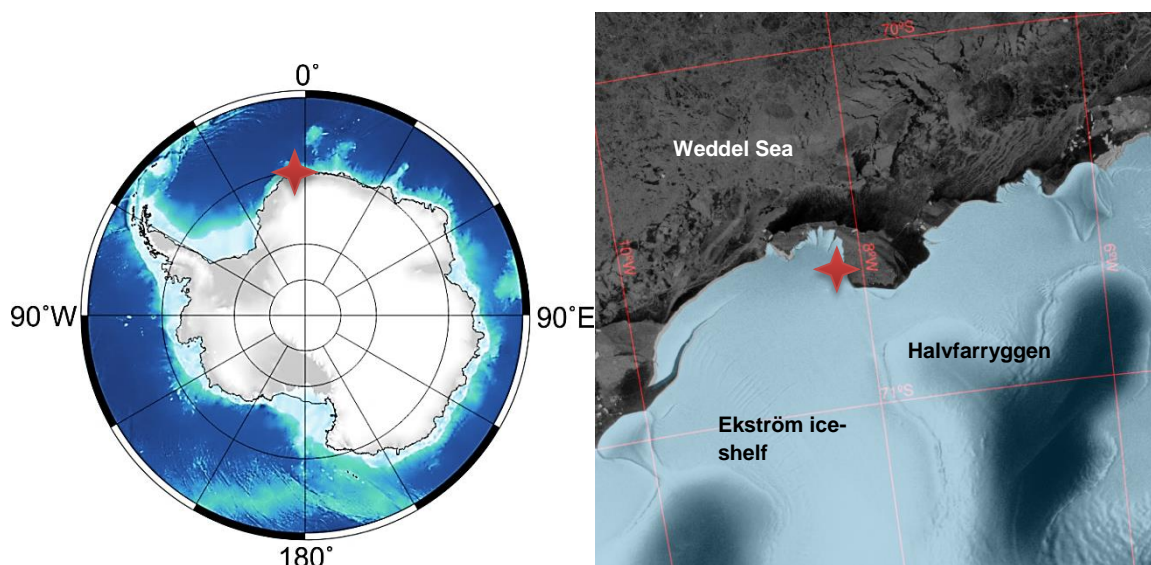


Figure 1.2: Bathymetric chart of the Antarctic (left) and Sentinel-1 image of the Ekström ice-shelf (right), adopted from Polar View ApS (Polar View, 2019). Neumayer Station is marked by a red star.

1.2 Previous studies of AIRS and IASI in the Antarctic

After commissioning a satellite, an individual validation report is prepared for each instrument as part of a calibration and validation phase, during which the performance of the instrument is extensively tested. There are various approaches to evaluate satellite data with data from other meteorological in-situ observations, due to fundamental differences between the measurements techniques. Methods differ broadly in terms of the satellite and in-situ measuring instruments used and their products, the spatiotemporal treatment of the data with respect to collocation and vertical resolution as well as in terms of the considered meteorological quantities. Hence, in the following section only some

of those approaches are introduced that are focused on retrieved satellite temperature profiles of the Atmospheric Infrared Sounder (AIRS) and the Infrared Atmospheric Sounding Interferometer (IASI).

The accuracy of AIRS and IASI derived temperature profiles in the Antarctic has been elaborated in validation reports (EUMETSAT, 2018 and Dang et al. 2017) and independent studies (e.g. Boylan et al., 2015, Boylan et al. 2016). AIRS and IASI atmospheric temperature profiles meet the NWP accuracy requirements of 1 K in 1 km layers on a global scale. Typically, the difference between radiosonde and satellite profiles tends to be larger in polar environments than on global average. The largest errors occur in the lowermost layers of the troposphere as well as in the tropopause. In general, the deviations vary for different locations in the Antarctic, such as the continental plateau, coastal, maritime or mountainous sites. The performance of satellite-derived products has never been evaluated for larger periods at one specific location. Furthermore, the quality of the retrieved products decreases with increasing cloudiness (EUMETSAT, 2018; Dang et al. 2017).

Evaluation of atmospheric profiles of AIRS and IASI in Polar regions by using higher resolution in-situ data e.g. radiosondes and dropsondes is performed by Boylan et al. (2015), Boylan et al. (2016), Wang et al. (2013) and Liu and Key (2006). In order to assess AIRS/IASI retrieval products, the highly resolved in-situ data are smoothed by applying averaging kernels, slab-layers (Feltz et al., 2017) or degraded to the satellite grid by vertical interpolation. Compared to dropsondes and radiosondes in the Antarctic on average, profiles of both, IASI and AIRS show slightly colder temperatures reaching its maximum in the lowermost troposphere. Furthermore, deviations between the sounders and in-situ measurements vary depending on the region of the Antarctic and the underlying surface (Boylan et al., 2015; Boylan et al., 2016, Wang et. al., 2013). Detection of temperature inversions is a challenge for the satellites, as the vertical resolution of the sounder may undercut the depth of an inversion. For the entire Antarctic, IASI and AIRS commonly underestimate the inversion intensity, whereas the depth and frequency of occurrence is overestimated (Boylan et al., 2015; Boylan et al., 2016).

Within the Antarctic, weather conditions vary greatly in space and time. For instance, characteristics of temperature inversions vary for coastal and continental sites as well as displaying seasonality (Zhang et al., 2011). Since the accuracy of satellite-based atmospheric profiles also varies on a global and regional scale (Boylan et al., 2015; Boylan et al., 2016), there is a special

necessity to evaluate satellite products for particular sites in Antarctica. As well as spatial variability, atmospheric conditions in Antarctica show rapid temporal change. Previous studies have not compared satellite observations with in-situ measurements at such a high sampling frequency as four times daily or for such a long time period as the entire polar summer. Past studies have focused on comparisons between satellite measurements and individual profiles (Boylan et al., 2015; Boylan et al., 2016, Wang et. al., 2013); however temperature time series of multiple satellite-derived data have never been performed.

This work is organized into six major sections. The introductory part of this work includes the theoretical background of meteorological satellite-based measurements. Section two deals with a data description of the different observational platforms used in this investigation, first the radiosonde measurements and second the infrared sounder of three polar-orbiting satellites. Section three presents and discusses the data post-processing scheme and introduces several statistical metrics. Section four shows the results. Followed by a discussion in section five, the final section summarizes the outcomes of the investigation where practical implications and limitations of the study are highlighted.

1.3 Theory of satellite measurements

Since the 1960s, meteorological atmospheric observations have been carried out by satellites. Meanwhile there is a broad network of geostationary and polar orbiting weather satellites, which permanently observe the Earth's atmosphere, oceans, vegetation and cryosphere on a wide range of the electromagnetic spectrum. Nowadays, the satellite radiances are assimilated by various weather and climate models and increase their forecast quality (Andersson et al., 1994). The majority of observational platforms do measure meteorological quantities in-situ. Remote-sensing techniques particularly satellites are fundamentally different, because all deduced meteorological information is based on received electromagnetic radiation. The following section describes the theoretical background of satellite measurements in accordance with the textbooks: Kidder and VonderHaar (1995) and Köpke and Sachweh (2012).

The origin of the remote-sensing measuring technology is Planck's discovery that matter emits energy in the form of electromagnetic radiation. The intensity of the emitted radiation varies with the wavelength and depends on the temperature of the matter. This relationship between emitted radiation of an idealized emitter,

wavelength and temperature is generally described by Planck's blackbody radiation (1) (Köpke und Sachweh, 2012a).

$$B_{\lambda}(T) = \frac{2hc^2}{\lambda^5 \exp\left(\frac{hc}{\lambda k_B T}\right) - 1} \quad (1)$$

Following Planck's law, the spectral emittance (B_{λ}) of a black body is controlled by its temperature (T) and wavelength (λ) as well as taking some natural constants into account, for instance the Planck constant (h), Boltzmann's constant (k_B) and the vacuum velocity of light (c).

Apart from the blackbody emission, there are additional interactions between matter, and electromagnetic radiation, such as emission, absorption and scattering. The interplay of all these processes determines the way radiation is transported in the atmosphere which is described by the Radiative-Transfer-Equation (RTE). Without going into too much detail, the complete RTE formulates the rate of change of radiation passing through an air volume which is dependent on four main processes involving absorption and scattering of the atmosphere's molecules (Köpke und Sachweh, 2012b). The full equation is adapted and restricted according to the intended use. In this case, we only focus on the Schwarzschild equation (2) that keeps the RTE very simple by neglecting scattering effects. As molecular scattering of molecules in the atmosphere in the infrared-range plays a minor role the Schwarzschild equation is a reasonable simplification.

$$\frac{dL_{\lambda}}{ds} = \sigma_a(s)(B_{\lambda}(s) - L_{\lambda}(s)) \quad (2)$$

The left hand side of the RTE represents the rate of change of a beam passing through the atmosphere. This is balanced by the right hand side, which includes two terms. The first term is a source of radiation describing the emission of radiation with respect to Planck's law and weighted by the volume absorption coefficient. The second term diminishes the ray by light absorption at molecules of the atmosphere determined by Lambert Beer's law. According to the Schwarzschild equation the intensity of a signal measured by a satellite depends particularly on: quantum mechanical properties of the molecules, temperature of the emitting bodies as well as concentration and distribution of gases of the atmosphere. This relationship allows temperature, water vapour and trace gases vertical profiles to be derived from satellites scanning the atmosphere at different wavelengths of the infrared spectrum (Köpke und Sachweh, 2012b).

To generate a vertical profile from received radiances the integrated version of the Schwarzschild equation (3) must be inverted. $\tau_0^{\mu^{-1}}$ is the slant-path transmittance from the surface (h_0) to the height of the satellite (h_{Sat}) and L_0 the radiation emitted by the Earth's surface. $W_\lambda(h, \mu)$ are the so-called weighting functions which balance the atmospheric term (Kidder and Vonder Haar, 1995a).

$$L_\lambda = L_0 \tau_0^{\mu^{-1}} + \int_{h_0}^{h_{Sat}} B_\lambda(T) W_\lambda(h, \mu) dh \quad (3)$$

$$W_\lambda(h, \mu) = \frac{d}{dh} (\tau_0^{\mu^{-1}}) \quad (4)$$

The signal received from a satellite consists of the sum of emissions from the Earth's surface and further contributions by the various altitudinal layers of the atmosphere, weighted by weighting functions. Each wavelength can be assigned to a weighting function. The function indicates at which part of the radiation it is transmitted at the corresponding wavelength and in the different atmospheric layers.

The shape and therefore position of the maximum of the weighting functions in the atmosphere are different for each wavelength. By scanning the atmosphere with many wavelengths (spectrum), vertical profiles of temperature, humidity and other trace gases can be generated. This processing step is carried out through retrievals. Since there are various approaches to run retrievals and in order to give an understandable overview, we will explain the functionality using a simplified scheme of an iterative physical retrieval computing a temperature profile described e.g. by Kidder and Vonder Haar, 1995b.

Step 1: Define the a priori background of trace gas profiles

Step 2: Choose a first-guess (FG) temperature profile

Step 3: Calculate the weighting functions

Step 4: Solve the RTE separately for each spectrometer channel (forward problem)

Step 5: Comparison of calculated and observed radiances

- ➔ Convergence: Calculated and observed radiances fit within spectrometer noise, thus the FG temperature profiles is accepted
- ➔ No convergence: FG profile is not accepted thus adjust FG and repeat step 3 to 5 until convergence is achieved

All retrieval procedures comprise of at least the five basic steps illustrated above. First, an a priori background has to be set containing estimated profiles of trace

gases which are infrared active such as CO₂, O₂ and H₂O among others. The a priori estimations of the trace gases are ordinarily generated using a climatological background (Kidder and Vonder Haar, 1995b). Subsequently, a first-guess temperature profile has to be chosen, thus weighting functions can be computed for each channel of the spectrometer (step 3) afterwards. In step 4, the forward problem is solved which means that for each channel the RTE is solved separately to get estimations of radiances the satellite instrument should have received with respect to the underlying initial conditions formulated in step 1 and step 2. Finally, the computed radiances are compared with the radiances measured by the satellite. If the computed radiances fit the measured spectrum within the range of the spectrometric noise convergence is achieved and the initially defined temperature profile is accepted. Otherwise, if the convergence criterion is not fulfilled the FG temperature profile has to be adjusted and step 3 to step 5 are repeated until convergence is achieved. A physical retrieval is not only used to retrieve temperature profiles but also to derive a wide range of other meteorological quantities, for instance trace gas profiles, including water vapour, cloud and surface properties. The main difference in the different cases is that for each variable a special set of channels is selected that is primarily sensitive to this variable. In addition, the initial conditions obviously need to be adjusted. It has to be noted, that the described retrieval scheme is a very basic example to explain the principle of a physical retrieval. However, a modern retrieval typically is instrument-specific and encompasses much more steps particularly when including multiple instruments, cloud-filtering/ cloud clearing methods or further statistical approaches.

In order to record the meteorological state of the atmosphere, modern satellite instruments operate primarily in the infrared (IR) or microwave (MW) range of the electromagnetic spectrum, called longwave. This has different reasons: On the one hand the natural shortwave radiation is strongly controlled by the sun, whereas upward longwave radiation comes predominantly from the Earth and the atmosphere. Hence, illuminating sunlight does not heavily impact the radiation received by the sounder in the longwave spectrum (Köpke and Sachweh, 2012b). Furthermore, there are strong absorption bands of well-mixed gases particularly in the IR range, for instance of CO₂ or H₂O. In these wavelength intervals the upward terrestrial radiation is dominated by these gases. Absorption bands that are sensitive to CO₂ and H₂O are therefore well suited for determining the atmospheric temperature profile, so the infrared sounders are focused to operate on these wavelengths. For this reason infrared sounder are indispensable to retrieve temperature and humidity profiles. Nevertheless infrared measurements are limited when sounding in cloudy scenes, because cloud droplets and aerosols strongly influence infrared radiation (Köpke and Sachweh, 2012b).

Hence, microwave sounders are supplementary used, since MW radiation is able to pass nearly unimpeded through non-precipitating clouds. Clouds are carefully treated in the retrievals due to cloud filtering or cloud clearing approaches or due to including MW measurements. The treatment of clouds and retrieval details are introduced in section 2.1.

Generally, Earth observing satellite sounders are measuring radiances directly. On their way to the end user remote-sensing raw data goes through different processing-steps. For the resulting intermediate products some established terms will be introduced (according to NASA, 2006):

Data of type Level 0 are unprocessed instrument and payload raw data, just as they are received by the sensing element. These are usually directly received detector signals with device-specific units. Level 1 data are reconstructed, time-referenced instrument data provided in physical units, annotated with ancillary information from the level 1 processing. The processing in particular includes radiometric and geometric corrections based on the sensor-specific calibration coefficients. Data of this type are for example brightness temperatures or integral and spectral radiances. Data that has undergone the level 2 processing are called level 2 data. As part of this processing stage geophysical quantities are derived from a single instrument in original instrument projection. In order to convert measured radiation quantities into geophysical quantities, the RTE must be inverted. This step is performed by a Retrieval process. Retrieved temperature profiles of type level 2 are the basis of our study. Nevertheless, following along the data-processing hierarchy level 3 data higher-grade products derived by level 2 data. Data of type level 3 are derived geophysical variables from a single-instrument mapped on a uniform, space and time grid, which does not necessarily fit the original spatiotemporal instrument projection. Finally the data of the highest-processing grade are of level 4. This data is modelled output or composite information derived from multi-sensors or different satellites (NASA, 2006).

2. Satellite and radiosonde data

2.1 Satellite observations

In this study we intend to generate a time series of temperature by assimilating retrieved satellite profiles of type level 2 from three different polar-orbiting satellites, namely AQUA, Metop-A and Metop-B. The selected satellites provide a good temporal coverage during the entire YOPP-SOP-SH (figure 2.2). The satellite profiles originate from measurements of the two highest-resolution hyperspectral infrared instruments, on the one hand AIRS as part of the AQUA satellite and on the other hand IASI which is placed on the Metop satellites. Both instruments are hyperspectral passive cross-track sounder, operating on similar wavelength intervals of the infrared electromagnetic spectrum (see table 2.1). They have several thousand channels and supply a comparable horizontal resolution at nadir. IASI and AIRS provide similar measuring precision of 1 K in 1 km layers regarding temperature and 10 % in 2 km layers in terms of relative humidity. So their vertical precision and accuracy meet the requirements of NWP (Aumann et al. 2003; Blumstein et al. 2004).

The quality of infrared soundings is substantially depends on the presence of clouds. Almost all incoming infrared radiation is absorbed by cloud droplets (Kidder and Vonder Haar, 1995a), so cloud contaminated radiances lead to a degraded quality of the profiles. However, there are different mechanisms to retrieve adequate temperature profiles such as cloud-clearing and cloud-filtering (Kidder and Vonder Haar, 1995a). On the other hand absorption processes are negligible in the microwave range of the electromagnetic spectrum, even in non-precipitating clouds (Goldberg et. al., 2003). Therefore, besides the IASI measurements, the Metop satellites additionally carry microwave-based instruments, for instance, the Advanced Microwave Sounding Unit (AMSU) and the Microwave Humidity Sounder (MHS) to be able to retrieve temperature profiles in cloudy situations with high accuracy. The AQUA satellite also carries analogous microwave instruments, but they have been deactivated due to sensing issues e.g. channel noises.

Table 2.1: Characteristics of AIRS and IASI (according to Aumann et al. 2003; Blumstein et al. 2004).

Instrument	AIRS (AQUA)	IASI (Metop-A, Metop-B)
Spectral intervals	3.7-15.4 μm (with gaps)	3.7-15.5 μm
Nadir resolution	13.5 km, for each 3x3 pixel	12 km, for each 2x2 pixel
Orbit height	705 km	817 km
Swath width	1850 km	2400 km
Cross-track samples	90	30
Channels	2378	8461
Maximum scan angle	$\pm 49.5^\circ$	$\pm 48.3^\circ$
Scan cycle	2.67 s	8 s
Vertical sampling of	100 temperature levels	101 temperature levels
L2 product	15 water vapour levels	100 water vapour levels
Nominal resolution	1 K / 1 km layer	1 K / 1 km layer
and stated accuracy	10 % / 2 km layer	10 % / 2 km layer

2.1.1 The infrared sounder IASI on Metop

The instrument IASI is a hyperspectral and passive across-scanning nadir sounder which is operated on the polar-orbiting, sun-synchronous Metop satellites (Metop-A and Metop-B), powered by the European Organisation for the Exploitation of Meteorological Satellites (EUMETSAT). IASI's technical properties are described in more detail in Blumstein et al. (2004) and are summarized in the following section. The Metop series were launched in 2006 (Metop-A) and 2012 (Metop-B). A third satellite Metop-C was launched 2018 but its data are not yet publicly available. The Metop satellites circumnavigate the Earth at an altitude of around 817 kilometres within approximately 100 minutes. Due to their orbital characteristics, a single location of the Earth's surface is observed at least once a day. A polar site e.g. Neumayer Station, is covered typically 2-4 times per day by each satellite. The key element of IASI is a Fourier Transform Spectrometer (FTS) which is based on a Michelson Interferometer whose functionality is explained in Blumstein et al. (2004). The FTS comprises of 8461 channels scanning continuously in the 3.7-15.5 μm infrared spectrum. Channels are focused on strong atmospheric absorption bands for instance, CO_2 , H_2O and O_3 as well as on the atmospheric transmission window, so ocean and land surface temperature, cloud properties, and trace gas profile can be determined. However, the probably most innovative aspect is the ability to provide temperature and humidity profiles in clear sky and in partly clouded sky conditions. Figure 2.1

illustrates the general setup of the IASI instrument. The sounder is designed to take 30 vertical samples within the entire measurement line, 15 to each side of the nadir angle. Each sample, so-called Instantaneous Field of View (IFOV) can be segmented into a 2x2 matrix of circular-shaped probes with a diameter of 12 km at nadir. The further the sounder probes are situated away from nadir angle, the more elliptical and larger the recorded footprint becomes. The full swath, meaning the ground measurement track, covers nearly 2400 kilometres.

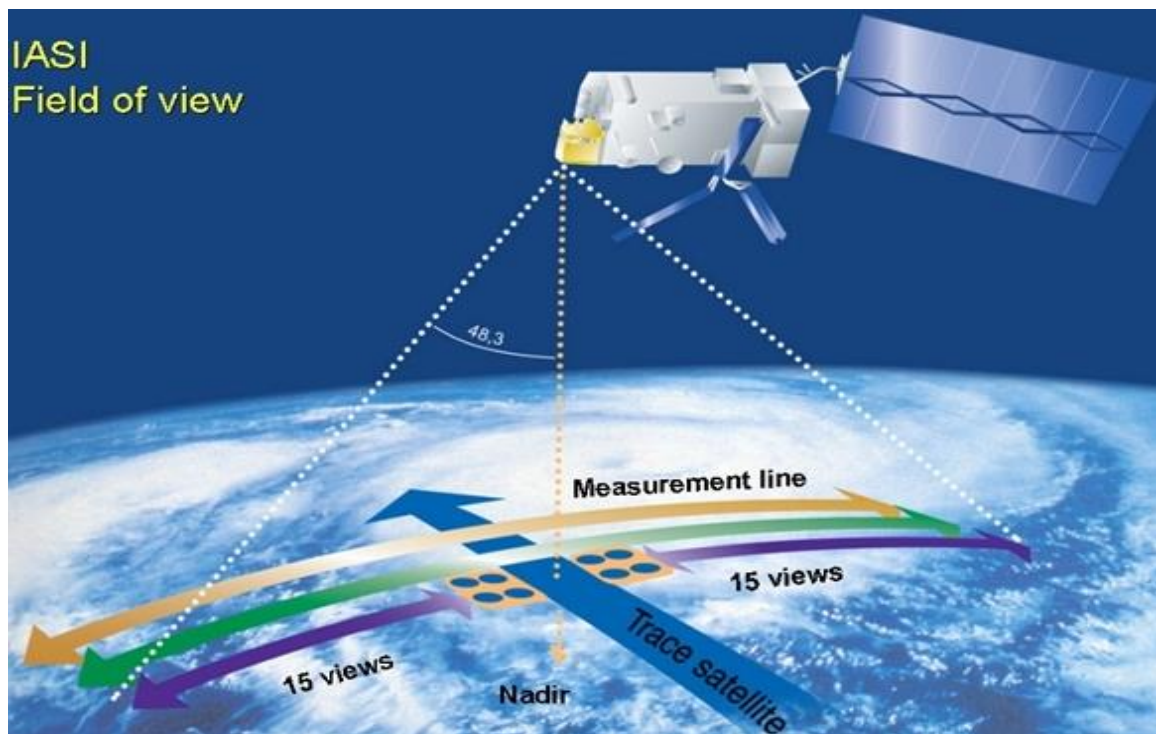


Figure 2.1: The instrument IASI on Metop, adapted from Hébert et al. 2017, figure 1.

IASI Level 2 products are generated by the so-called IASI Level 2 Processor (Schlüssel et al. 2005). As a first statistical retrieval, a Piece-Wiese Linear Regression Cube (PWLR³) is performed. The PWLR³ also includes measurements from Metop's AMSU and MHS instruments and provides the FG profiles for all-sky conditions. If no appropriate collocated MW information is available e.g. due to large channel noises, the PWLR³ is run in a specific IR-only mode (Hultberg and August, 2013). The statistical retrieval is followed by a cloud filtering step in which Advanced very high resolution radiometer (AVHRR) radiances and NWP forecasts are exploited only for cloud-detection purposes (EUMETSAT, 2017b). The cloud-detection algorithm decides whether a profile is expected to be cloud contaminated or cloud-free. If the influence of clouds is assessed to be negligible, temperature profiles are determined by an optimal estimation method (OEM) retrieval, which involves the PWLR³ FG as a-priori profile. Apart from the FG input, the OEM retrieval is purely based on IASI radiances in predominantly cloud-free or clear scenes. As the FG retrieval and

the OEM retrieval are purely based on radiances and climatological reanalyses, the output temperature profiles are fully independent from the YOPP-SOP-SH radiosondes and current forecasts.

2.1.2 The infrared sounder AIRS on AQUA

As part of the so-called “A-Train” the National Aeronautics and Space Administration (NASA) operates the sun-synchronous, polar-orbiting AQUA satellite which was launched in May, 2002. On its orbit, AQUA is placed at an altitude of 705 km above the Earth’s surface and each orbit last about 100 minutes. The satellite carries a wide range of sensing instruments to collect information about the oceans, the cryosphere, the lithosphere as well as the atmosphere (Parkinson, 2003). Concerning the atmospheric part AIRS central objective is to provide highly accurate temperature and trace gas profiles. Details about AIRS’ technical design and instrument characteristics can be found in Aumann et al. (2003) and are summarized in the following section. AIRS is a high-resolution, passive crosstrack-scanning nadir grating spectrometer, sounding the atmosphere by using 2378 IR channels. Although AIRS’ channels are concentrated on particular absorption bands between 3.7 and 15.4 μm , but they do not distribute homogeneously all over the spectral interval. Nevertheless, the covered spectral range coincides with IASI. The full swath amounts to about 1850 km and includes 90 cross-track samples which are recorded within 2.67 seconds. Each sample contains a 3x3 footprint which has a horizontal diameter of 13.5 km at nadir. As AIRS’ technical design, horizontal resolution and coverage are similar to IASI, AIRS also reaches a comparable nominal accuracy for retrieved temperature and humidity profiles (table 2.1).

In this study, temperature profiles are assimilated which are purely derived from AIRS measurements. The core of the corresponding AIRS-only retrieval rests on a physical retrieval containing the 5 basic steps (section 1.2). Previous to the physical retrieval two more pre-processing steps are implemented in which the FG is generated by performing cloudy and clear regression on AIRS measurements as well as clear-column radiances are produced (Susskind et al., 2003). It has to be noted, that the first-guess is generated by using cloud cleared AIRS measurements and a neural network (NN), which was trained by assimilating ECMWF analysis fields spanning from December 2004 to January 2006 (Millstein and Blackwell, 2016). The AIRS-only retrieval product therefore is independent from the YOPP-SOP-SH radiosonde data and current forecast products of NWP models. Details about the NN approaches can be found in Millstein and Blackwell, 2016 and Tao et al., 2013.

2.1.3 Data access and availability

Concerning IASI profiles, the product “IASI Atmospheric Temperature Water Vapour and Surface Skin Temperature – Metop” is assimilated via EUMETSAT’s Earth Observation Portal (EOP) (©EUMETSAT, 2019). This product can be requested at <https://navigator.eumetsat.int/start>, and consist of retrieved FG temperature profiles derived from IR and MW radiances in all-sky conditions and from pure IASI radiances when cloud contamination is expected to be negligible. To ensure comparability with the AIRS dataset we only use IASI profiles which are retrieved by pure IASI measurements for hardly clouded or cloud-free pixels. This limitation leads to a fewer availability of profiles for instance in stormy conditions where deep, precipitating clouds are dominant (see figure 2.2). The parameter names of the assimilated product are given in parentheses. Apart from the temperature profiles (atmospheric_temperature), which are represented on 101 predefined pressure levels, quality indicators as well as geolocation fields are given (EUMETSAT, 2017a). The geolocation fields contain the horizontal grid and also temporal information. The surface pressure is accessed from ECMWF forecasts and adjusted by a Digital Elevation Model (DEM) which takes the topography of the IFOV into account. The surface pressure is used as input for the level 2 processing. The surface pressure (surface_pressure) and the surface skin temperature (surface_temperature) are then separate outputs from the OEM retrieval and independently provided from the retrieved profiles (EUMETSAT, 2017a; EUMETSAT, 2017b).

The second source for satellite data is the product “AIRS Aqua L2 Support Retrieval (AIRS-only) V006” of the Goddard Earth Sciences Data and Information Services Center (GES DISC) funded by NASA’s Science Mission Directorate (SMD) which is available at <https://disc.gsfc.nasa.gov> (AIRS Science Team/Joao Teixeira, 2013). The product contains atmospheric temperature profiles on 100 pressure levels (TAirSup). The pressure levels (pressSup) correspond to the lowermost 100 of IASI’s levels and are result from a vertical linear interpolation of the retrieved profiles (AIRS Version 6 Level 2 Product Guide). Besides that, surface pressure and surface temperature not a directly generated by the AIRS retrieval. The surface pressure (PSurfSTD) is a first guess generated by interpolation from the National Centers for Environmental Prediction (NCEP) Global Forecast System (GFS) and corrected by a DEM. The surface temperature (TSurfAir) TSurfAir is derived using vertical interpolation of the TAirSup profile to the surface pressure (AIRS, 2017a). Apart from the meteorological quantities, also geolocation fields, swath attributes and quality flags as ancillary data are content of the accessed product.

The retrieved AIRS and IASI temperature profiles are provided on a fixed vertical grid of about 100 predefined levels, of which only 76 are used in the present analysis, which lie between the surface and the stratosphere (~12.5 hPa or 30 km). On principle, the sounding products are representing the meteorological conditions on layers on a certain vertical extend by processing radiation information captured at the top of the atmosphere (EUMETSAT, 2017b). Hence, the definition of the fixed layers has to be taken with caution since their altitude varies with the synoptic situation and furthermore exceeds the vertical sampling capabilities of the satellite instruments. All profiles used in this work should be regarded as an output of the level 2 processing in which vertical interpolations are made to construct temperature on a finer grid. The vertical interpolation schemes of the level 2 processing are documented in EUMETSAT, 2017a and in AIRS, 2017b.

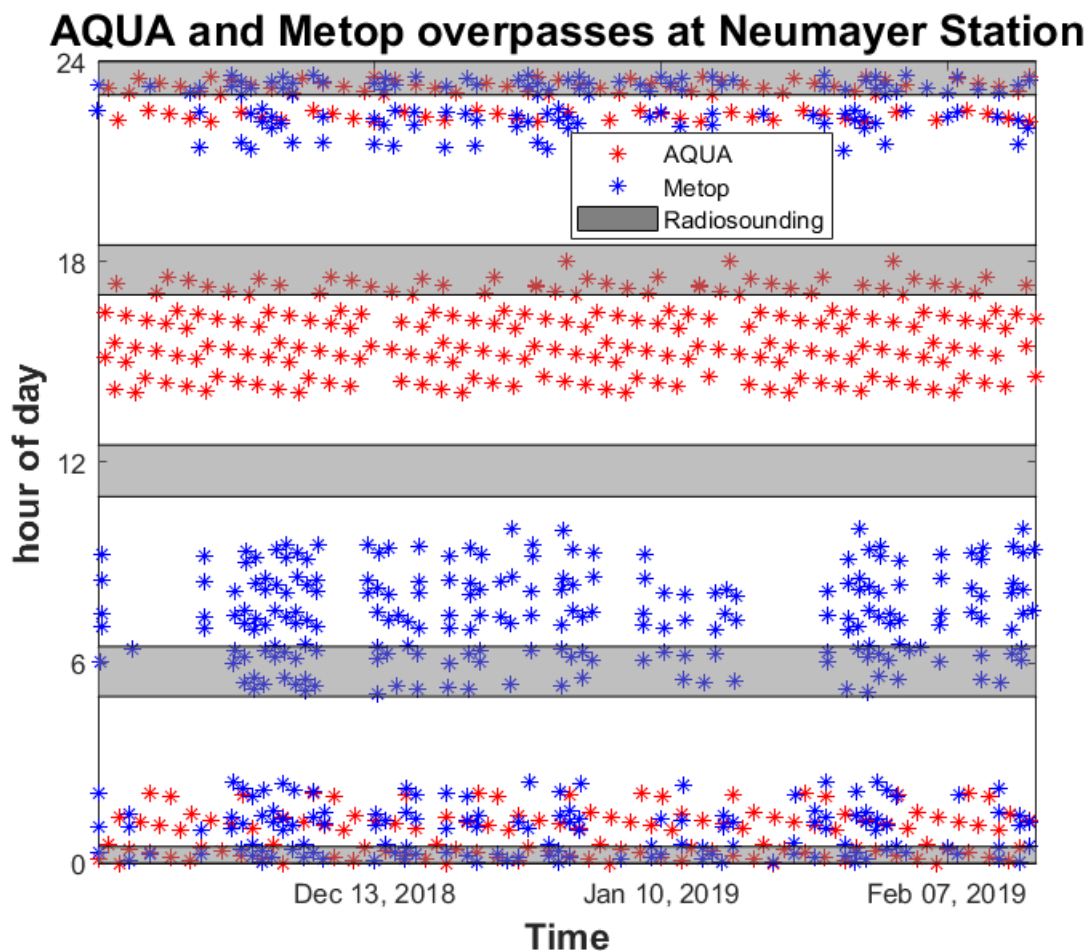


Figure 2.2: Availability of AIRS and IASI data during YOPP-SOP-SH. Collocated AQUA (red), Metop-A and Metop-B (blue) overpasses within a circle of 50 kilometres around Neumayer Station. The grey bars represent the regular radiosonde measurement intervals.

Temporal coverage of AIRS and IASI differs, since the orbits of the three satellites are different. Figure 2.2 illustrates the availability of IASI and AIRS measurements after spatiotemporal collocation and quality control during YOPP (section 3.1). Obviously, the usage of both, Metop and AQUA data is of fundamental importance to cover the whole day by satellite observations. At Neumayer Station, AQUA and Metop overpasses are regular between 22 and 03 UTC of each day, so the 00 UTC radiosonde ascents is captured very well. Metop overpasses appear frequently around 05 and 10 UTC and are most important for the 06 UTC launch as there are no AQUA observations. Later in the day, the 18 UTC is covered predominantly through AIRS observations which occur between 14 and 18 UTC. Thus, the 12 UTC is never captured directly by the satellites. A noticeable feature of figure 2.2 is the irregularly appearing data gaps of IASI profiles. The IASI retrieval is only performed, if the cloud fraction is expected to be negligible (cloud-filtering), whereas the AIRS-only retrieval attempts to produce clear-column radiances for clear spots of cloudy scenes (cloud-clearing). Hence, the data gaps can be associated with heavily clouded scenes, in which the IASI retrieval is not performed.

2.2 Radiosonde observations

2.2.1 Vaisala RS41-SGP radiosondes

During the entire Special observing period of the WMO's YOPP in the Southern Hemisphere between Nov., 16th 2018 and Feb., 15th 2019 in total 339 radiosonde launches have been carried out at the four synoptic main standard times, i.e. 00, 06, 12 and 18 UTC at Neumayer Station. The launches were performed approximately one hour before the synoptic main standard time, to ensure that the radiosondes cross the 100 hPa level roughly at the main times. The RS41-SGP radiosondes are manufactured by Vaisala (Finland) and consist of different battery-driven sensing instruments to capture essential meteorological quantities with a sharp measuring precision. A radio transmitter instantly transfers the measured data to the ground station. Temperature, relative humidity and pressure are measured directly by specific sensors, while a GPS receiver records the geographical coordinates to derive information concerning wind, height and pressure as well. In general, each variable is recorded at least once within a one-second measurement cycle. The measurement precision of each sensor or derived parameter is given in table 2.2.

The temperature measurements are based on a resistive platinum sensor, which records temperature with an accuracy of 0.4 °C within the entire profile. Furthermore, a thin-film capacitor is measuring relative humidity with a combined uncertainty of about 4 % in the whole sounding. The humidity sensor design contains a heating resistor which prevents icing of the sensing elements. Regarding pressure measurements, there are different methods used to produce pressure information. Pressure is recorded directly by a capacitive silicon sensor with combined measuring precision of about 1.0 hPa up to the 100 hPa level and 0.6 hPa between 100 hPa and 3 hPa. On the other hand, pressure data is also calculated by the ground station using hydrostatic approaches which include measured temperature, humidity and GPS-based height information. Further details about the pressure derivations are documented in Vaisala, 2013b. The hydrostatic based pressure and height values are used for the analysis. Both, wind direction and wind speed are derived separately through the GPS-data by the ground station. High-quality results of wind speed and direction are implemented by the Vaisala DigiCORA® Sounding System MW41 with an uncertainty of 0.15 ms⁻¹, respectively 2° in terms of directional wind measurement accuracy (Vaisala 2013a).

Table 2.2: Sensors and uncertainties of Vaisala’s radiosonde RS41-SGP (according to Vaisala, 2018).

Sensing element (variable)	Combined uncertainties
Platinum Resistor (temperature)	0.3 K in sounding < 16 km 0.4 K in sounding > 16 km
This-Film Capacitor (relative humidity)	4 % in entire sounding
Silicon Capacitor (pressure)	1.0 hPa in sounding < 100 hPa 0.6 hPa in sounding > 100 hPa
GPS-derived wind speed	0.15 ms ⁻¹ in entire sounding
GPS-derived wind direction	2° in entire sounding

Each radiosonde was attached to a helium-filled balloon manufactured by Totex, Type TX600, TX800 or TX1500. The balloon was filled with helium that an average ascent rate of nearly 5 ms⁻¹ is reached to guarantee that the sensing elements are sufficiently ventilated. Prior to the start-up process, a ground preparation was carried out automatically by the ground station to ensure that all sensors are functional and do work properly. As part of the ground check both, temperature and humidity sensors were examined separately, and the pressure sensor was calibrated with a reference pressure sensor included in the ground station. Only if the calibration check is accomplished successfully for each sensor, the sonde was launched.

After the sonde has been successfully started, the current weather conditions must be entered in the sounding unit as the surface values at the time of the start. These are recorded at the meteorological field that is located about 400 meters away from the launch platform. As initial values therefore, we use the temperature and humidity measurements 2 meter above the surface, and the 10 meter wind speed and wind direction. The balloons were started on the roof of Neumayer Station that is elevated 68 metres above the sea level and around 25 metres above the station level. It is to be noted that the initial entries of a profile do represent parameters recorded by the meteorological field although they are given for a height of 25 metres above the surface. The subsequent entries refer to data which are directly recorded by the sonde. In addition to the surface value input a brief visual synoptic cloud observation is carried out, so information of both, local cloud coverage of low and medium clouds and observed dominant cloud types is attached to metadata of each profile. After the balloon had burst, the measuring process was aborted and the recorded profile was transferred directly to the meteorological network GTS.

2.2 Data access and availability

Table 2.3: Radiosonde ascent statistics. Mean and standard deviation of pressure, ascent time, drift and number of sondes for some altitude levels.

Altitude [m]	Pressure [hPa]	Ascent time [min]	Horizontal drift [km]	Sondes [#]
Launch level	975.12 ± 6.59	0.00 ± 0.00	0.00 ± 0.00	339
1000	857.98 ± 6.01	3.09 ± 0.25	2.22 ± 1.45	339
2000	752.95 ± 5.54	6.18 ± 0.50	4.02 ± 2.62	338
5000	499.92 ± 5.34	15.26 ± 1.14	8.10 ± 5.19	338
10000	235.67 ± 3.85	30.42 ± 2.39	15.22 ± 10.75	338
15000	109.99 ± 2.66	46.86 ± 3.96	19.80 ± 14.96	337
20000	52.24 ± 1.95	62.73 ± 4.80	22.79 ± 18.42	333
25000	25.20 ± 1.06	77.18 ± 5.76	26.01 ± 21.67	327
30000	12.36 ± 0.40	90.53 ± 6.86	28.27 ± 22.79	311
35000	6.14 ± 0.15	116.22 ± 10.53	31.70 ± 21.76	17

The radiosonde profiles used for the this work are publicly available and requested from the Pangaea data base (Schmithüsen and Müller, 2019 a,b,c; Schmithüsen and Koch, 2019). Although these data have gone through a validation routine, the assimilated profiles are subjected to a further quality check. For our study, we formulate specific selection criteria that decisively determine whether a radiosonde is used for the analysis. Details of the quality check and

the selection criteria will be described in section 3.1. Because of extreme weather situations or instrument failures only 339 radiosonde ascents of the 368 intended measurements during the field campaign are used in the analysis. 28 radiosonde observations have not been conducted due to heavy storms. Two measurements are rejected because of instrument issues. For the remaining radiosondes profiles ascent statistics are calculated which can be found in table 2.3. In fact, numbers of drift, pressure and ascent duration vary significantly with synoptic weather situations. For instance, the horizontal drift during ascent is driven by the current tropospheric and stratospheric winds (see figure 2.3). Thus, the range of horizontal drift extends from only a few kilometres to more than 100 kilometres in extreme cases. Therefore, all numbers refer to the arithmetic mean and its standard deviation. In summary, the major part (about 92 %) of the radiosondes reaches altitudes above 30000 m above the sea-level, respectively 12.36 hPa, so in this study we focus on a comparison from the surface up to this elevation. On average, the full radiosonde ascent up to this level lasts about 90 minutes while the instruments experience a mean horizontal drift of nearly 28 km. The computed ascent statistics are essential to define reasonable collocation criteria (see section 3.2).

Radiosonde tracks at Neumayer Station

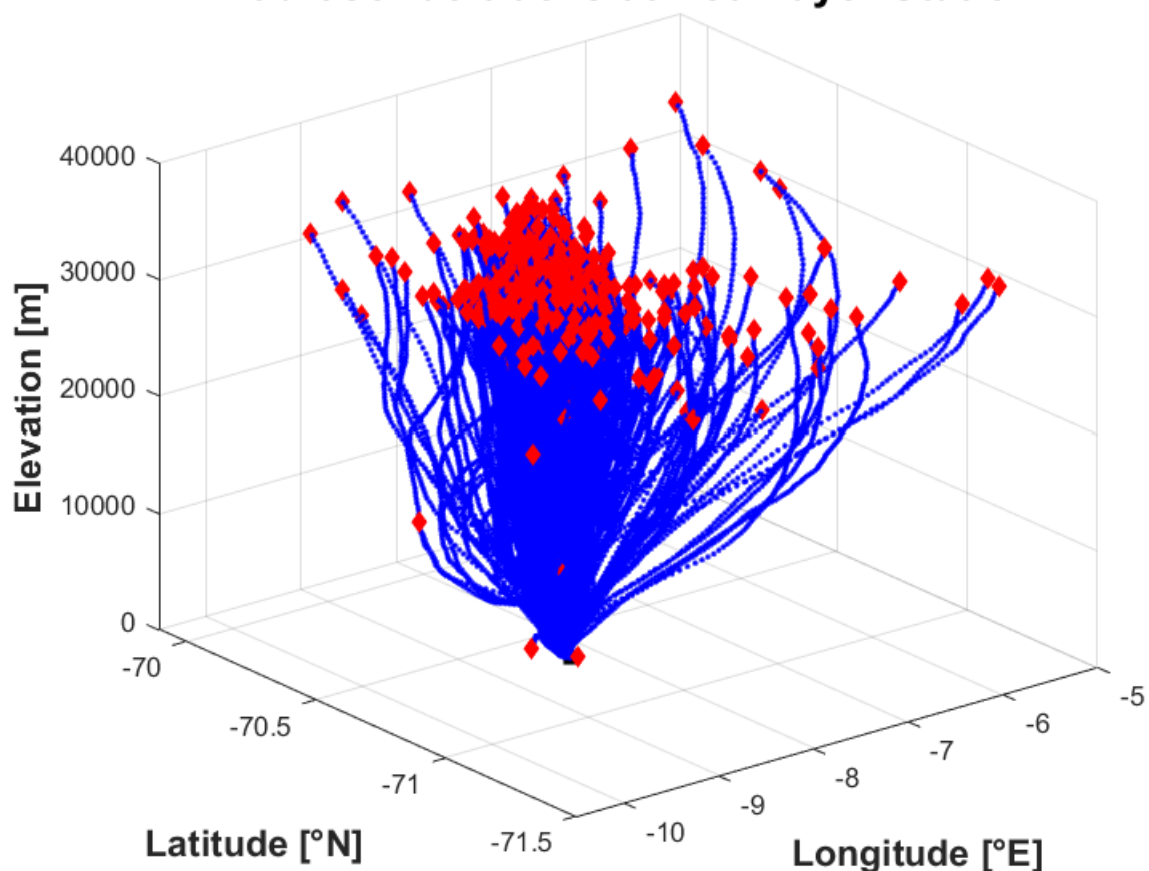


Figure 2.3: Radiosonde ascent tracks (blue) at Neumayer Station during the YOPP-SOP-SH. The points of balloon bursts are highlighted red.

3. Methodology of data processing

3.1 Data processing scheme

As radiosonde and remote-sensing techniques are fundamentally different, this section describes how to find the most appropriate way to compare profiles from these observational platforms with each other. Table 3.1 gives a tabular overview of the key disparities of radiosonde and satellite data. A polar site is passed several times per day by a polar-orbiting satellite. Each retrieved satellite profile represents a nearly vertical insight into the atmosphere at one specific point in time. On the other hand, each individual radiosonde ascent takes around 90 minutes to reach the mid stratosphere, so the recorded observations are not necessarily representative for one particular point in time. Additionally, the individual retrieved satellite profiles can be considered as cylindrical atmospheric columns where each column is allocated to a small spot with a diameter of only few kilometres on the Earth's surface. On the contrary, the horizontal movement of the radiosondes during their ascent is driven by wind, and therefore individual for every launch. Thus, the horizontal displacement of the radiosondes during ascent may exceed the size of a single satellite footprint leading to a potential spatial mismatch. To deal with the spatial and temporal issues, we implement a special data processing scheme illustrated by figure 3.1.

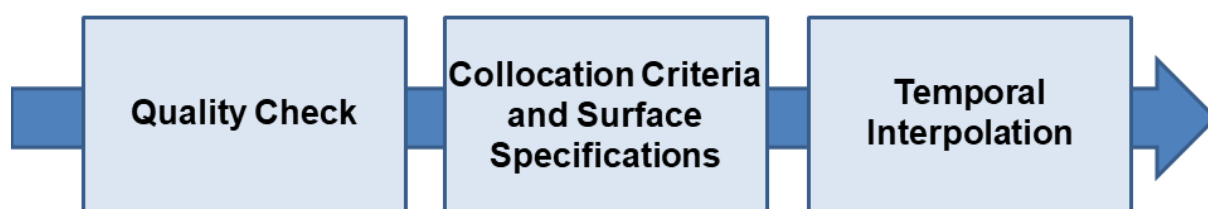


Figure 3.1: Overview of the three steps of the data processing.

Table 3.1: Key disparities of radiosonde and satellite measurements.

	Radiosonde measurements	AIRS & IASI measurements
Technique	In-situ (direct measurement)	Space-borne (retrieved process)
Data gaps	Early balloon bursts, Instrument failures	Data gaps in cloudy-situations, Instrument failures
Measuring property	Point measurement	Average over a pixel of at least 450 km ² horizontal extent
Horizontal range*	Horizontal drift up 120 km	Nearly vertical profile
Duration of observation	Ascent lasts about 90 minutes	Entire profile at one point in time
Frequency of observation*	4 times daily	Number of available profiles between 2 and 10
Vertical Resolution	About 5 m	About 1 km

*At Neumayer Station during YOPP

3.1.1 Quality check

The primary purpose of the quality check is to guarantee that in our analysis only data of best quality are used. In order to ensure this, we formulate specific requirements separately for both, satellite and radiosonde measurements that have to be fulfilled.

Radiosonde data post-processing

During the measuring process diverse issues may occur for instance, sensing problems, loss of GPS connection and recording of unphysical values. Thus, each individual radiosonde profile has to fulfil the following quality requirements.

1) For the comparison we use radiosonde profiles only, which have reached elevations of at least 10000 metres above the sea-level, according to the GPS-based height records of the radiosondes. Furthermore, each radiosonde profile must not contain information gaps extending over 100 metres and more. In total three radiosonde profiles are rejected because they do not meet these requirements.

2) Errors in the measuring process may lead to so-called unphysical values e.g. a negative relative humidity. These values merely appear isolated and are filtered

out. None of the radiosonde profiles contain a considerable number of unphysical values, so no entire profile is rejected due to unphysical-value detection. An exception of this is the launch on the 27th November 2018 at 06 UTC. The radiosonde carried an obviously broken temperature and humidity sensor. Because this sonde lost its GPS connection at an elevation of 1296 m, the profile does not fulfil the previous criteria and is rejected anyway.

The radiosonde profiles which satisfy both criteria are vertically interpolated onto a fine pressure grid of 0.01 hPa grid size from the surface up to 12.36 hPa, which on average corresponds to about 30 kilometres. Those radiosondes that did not reach that 30 km a.s.l. are interpolated only up to the level of the balloon burst. Hence, there is no extrapolation beyond the original vertical range of the radiosonde profiles.

Satellite data post-processing

The quality of retrieved satellite profiles basically depends on cloud contamination and instrument noises during the measuring process. For each parameter of the retrieved products, AIRS and EUMETSAT provide quality indicators Q ranging between best (Q=0) and worst quality (Q=2). In order to guarantee high quality of the AIRS and IASI profiles, the quality indicators are used to determine whether to use or to reject a profile. Since EUMETSAT's clear sky, OEM retrieval is exclusively started, if all measurements are of acceptable quality, the derived profiles are entirely flagged with best accuracy (EUMETSAT, 2017b). On the other hand, the AIRS-only, all-sky retrieval is performed for all quality flags. Following the manufacturer's recommendations we select all AIRS-only temperature values which are flagged with best (Q=0) and good (Q=1) quality (AIRS, 2017a).

3.1.2 Collocation criteria and surface adjustments

Atmospheric temperatures vary not only vertical but also on a horizontal scale. As satellite footprints never spatially coincide with radiosonde measurements, strict criteria of spatial collocation are required for a reliable analysis. Representativeness of satellite profiles is expected to be at largest, if the horizontal distance between collocated IFOV and the radiosondes is minimal, which is given by narrow thresholds of collocation. Too much limitation, on the

other hand, leads to a reduction in the number of collocated satellite profiles. Spatial collocation of both, radiosondes and satellites have been performed by several recent studies by different criteria. Selection criteria range predominantly between 100 km (e.g. Divakarla et al., 2006, Pougatchev et al., 2009) and 250 km (e.g. Reale et al., 2012). However, Neumayer Station is located within the polar circle and data of three polar-orbiting are used, so a large number of available profiles is expected. This offers the opportunity of setting strict thresholds without substantial loss of data.

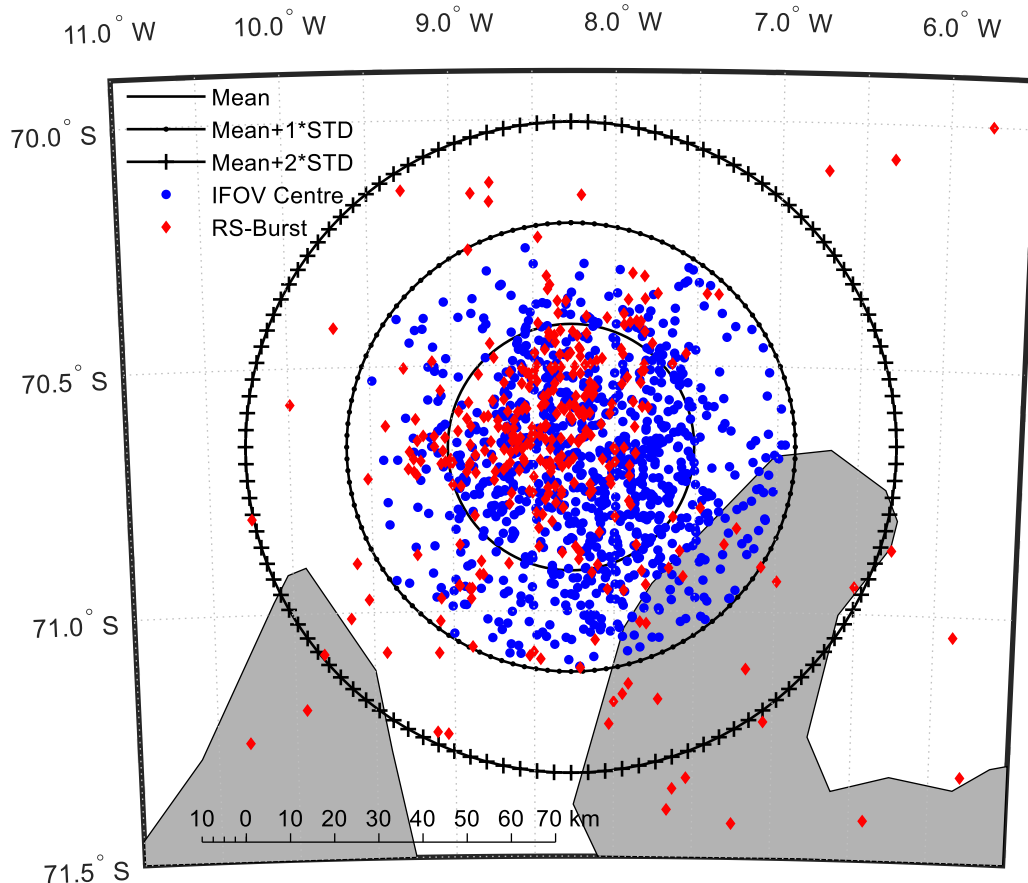


Figure 3.2: Birds-eye view for the northern edge of the Ekström ice-shelf. The black circles show different distances to Neumayer Station based on the radiosonde drift computations. Neumayer Station is located in the centre. The red diamonds represent the balloon burst locations while the blue circles indicate the IFOV centre of collocated satellite measurements. The shelf-ice is not visible in this illustration. The grey shaded are indicates the Antarctic continent.

The spatial collocation criterion of our study is formulated according to the computed radiosonde drift statistics (section 2.2). As we focus on the lowermost 30 kilometres of the atmosphere, on average the radiosondes drift about 28 kilometres away from Neumayer Station with a single standard deviation of

almost 23 kilometres. Therefore, within a circle of 51 kilometres around the Station we select the nearest available satellite footprint (see figure 3.2).

A separate collocation criterion is implemented exclusively for surface temperature which is an independent variable in the products. If we take into account the geographical location of Neumayer Station, the season and the size of the footprints, the nearest match is not necessarily the most representative. For instance, a footprint located 20 kilometres to the north of the station would receive radiances which are influenced by open water and closed or partially broken sea ice which does not fit the surface conditions at Neumayer Station. That issue would lead to large differences of the surface parameters because e.g. surface temperatures are typically higher over water than at the surface of the ice-shelf. Hence, to increase the representativeness of the satellite-based surface parameters, we select the closest footprint within the 51 kilometre circle located to the south of Neumayer Station for the surface value. As the territory to the south of the site is very flat and homogeneous, this approach should be justifiable. Surface value and profile are collocated independently from each other. The surface value is attached to the collocated profile by its associated surface pressure. Applying the different collocation filter on the Metop and AQUA measurements, in total 916 satellite profiles can be collocated in the entire YOPP period corresponding to about 10 per day. In fact, this number varies from day to day since availability of IASI data depends on the underlying cloudiness. Note, that there are days which are captured by two satellite overpasses only.

3.1.3 Interpolation of the radiosonde and satellite data

This section deals with the vertical processing and temporal interpolation of satellite and radiosonde measurements. In order to find the most appropriate way to compare radiosonde and satellite time series with each other, several methodologies are investigated.

Temporal interpolation

The key goal of the temporal interpolation is to bring radiosonde and satellite measurements at the same time. There are three possible approaches to bring radiosonde and satellite measurements on the same times:

1. A linear temporal interpolation of the satellite profiles on the respective radiosonde measuring times: In this approach, no restrictions are set, so a new satellite profile is constructed on the basis of the temporally surrounding collocated profiles. It is worth mentioning that a newly designed satellite profile may contain information from different sensors. For instance, a constructed satellite profile for 12 UTC e.g. would be constructed by the two nearest satellite products in time, usually from the Metop profile in the morning and the AQUA profile in the afternoon. The respective IASI and AIRS components that make up the designed profile basically depend on the temporal difference between the radiosonde measurement time and the overpass time of the satellites.

2. The radiosonde profiles could be also temporally interpolated on the satellite overpass times, so a newly constructed radiosonde profile could be assembled to single AIRS or IASI measurements. This approach would have two major disadvantages: On the one hand particularly in cloudy situations where the availability of satellite observations is sparse, the course of a day would not be covered, so some radiosonde ascents may be redundant. Additionally, a 12 UTC radiosonde profile would never be generated because this time is not captured by the Metop and AQUA at Neumayer Station (figure 2.2). Additionally, since we want to extend the analysis in the representation of surface inversions by the satellites it is not beneficial to smear the sharply resolved radiosonde profiles by performing a temporal interpolation.

3. As a third method, temporal interpolations of satellite and radiosonde measurements could be conducted on a fixed temporal grid covering the entire day in regular intervals by the four main synoptic standard times at 00, 06, 12 and 18 UTC. Compared to the second approach the entire day would be covered homogeneously. However, this approach also generates a loss of sharp meteorological structures measured by the radiosondes due to the temporal interpolation.

The only restriction which is set for all three approaches is that we do not extrapolate satellite and radiosonde data beyond their original temporal range which means that at times of missing radiosonde ascents no comparison is elaborated.

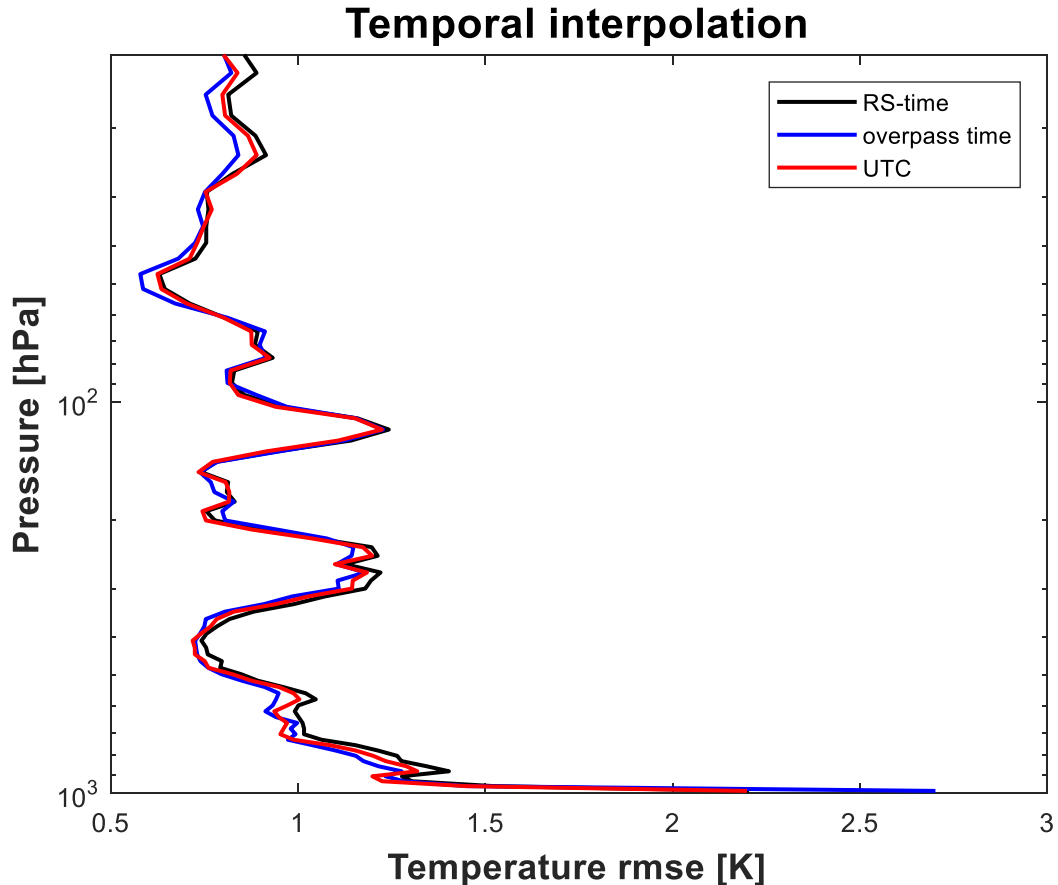


Figure 3.3: Comparison of the three methods of temporal interpolation. Interpolation of satellite profiles to the radiosonde measurement times (first approach, black line), radiosonde data interpolated to satellite overpass times (second approach, blue line), and temporal interpolation of satellite and radiosonde measurements to the synoptic standard times (third approach, red line).

In figure 3.3 the temperature root-mean-square-error (rmse, definition in section 3.1.4) on average for the whole observing period is presented for the three different temporal interpolation methods. A key statement of figure 3.3 is that none of the different temporal interpolation approaches clearly indicates a significant smaller rmse. Therefore, to maintain the meteorological conditions as recorded by the radiosondes, a temporal interpolation of the satellite profiles on the radiosonde point measurements (approach 1) is preferred in the following analysis.

Vertical approaches

Temperatures are given on 100 predefined vertical pressure levels of which 76 are within the lowermost 30 kilometres. The vertical resolution of the radiosonde

profiles is several times higher compared to the vertical sampling of the satellite sounders. Thus, according to the theory of satellite retrievals (section 1.3) and literature (section 1.2) there are various possibilities to compare the profiles. Two basic approaches are introduced:

1. The primal and probably the most intuitive approach would be a “line-to-line” comparison of radiosonde and satellite data on the predefined pressure levels of the satellite support product. Hereby, each radiosonde profile would have to be degraded on the satellite product grid by interpolating the quantities to the vertical satellite grid.

2. Common approaches deal with a vertical degradation of radiosonde temperature profiles by applying weighted averages or averaging kernels. As they contain information concerning the vertical sensitivity and smoothing of a retrieved quantity, AKs are used to degrade higher-resolution profiles to the resolution of sounder (e.g. Feltz et al., 2017). The shape of the averaging kernels is individual for every instrument and varies with atmospheric state. The generated satellite time series of this study is compounded of different retrieval products which are interpolated in time, so no particular kernel can be assigned to a single radiosonde observation. To demonstrate the effect of smoothing the radiosonde data, we provide an exemplary degraded radiosonde profile which is vertically smoothed by a (Gaussian) weighted average corresponding to the vertical sounder resolution of 1 km (figure 3.4).

Figure 3.4 illustrates the effect of applying a vertical smoothing to the radiosonde data. Meteorological structures which are typically characterized by a limited vertical extent such as tropopause and temperature inversions are blurredly represented. The temperatures of tropopause are overestimated while in the lowermost tropospheric levels the satellite products tend to underestimate the radiosonde measurements. Small temperature fluctuations e.g. in the mid troposphere and in the stratosphere are also not captured by the smoothed curves (figure 3.4a). The profile of the root-mean-square error (defined in section 3.2) demonstrates that rmse is smaller for the smoothed profiles. Nevertheless, the shape of both curves is very similar for wide parts of the profile (figure 3.4b). Performing a smoothing is reasonable to give the retrieved satellite profiles a fair chance to represent the current state of the atmosphere. However, we prefer the “line-to-line” comparison of temperature profiles, because a vertical interpolation of the radiosonde data to the 76 levels of the satellite products should be closer to the true physical state of the atmosphere. Smoothing of the in-situ data to coarse layers particularly leads to a loss of meteorological information.

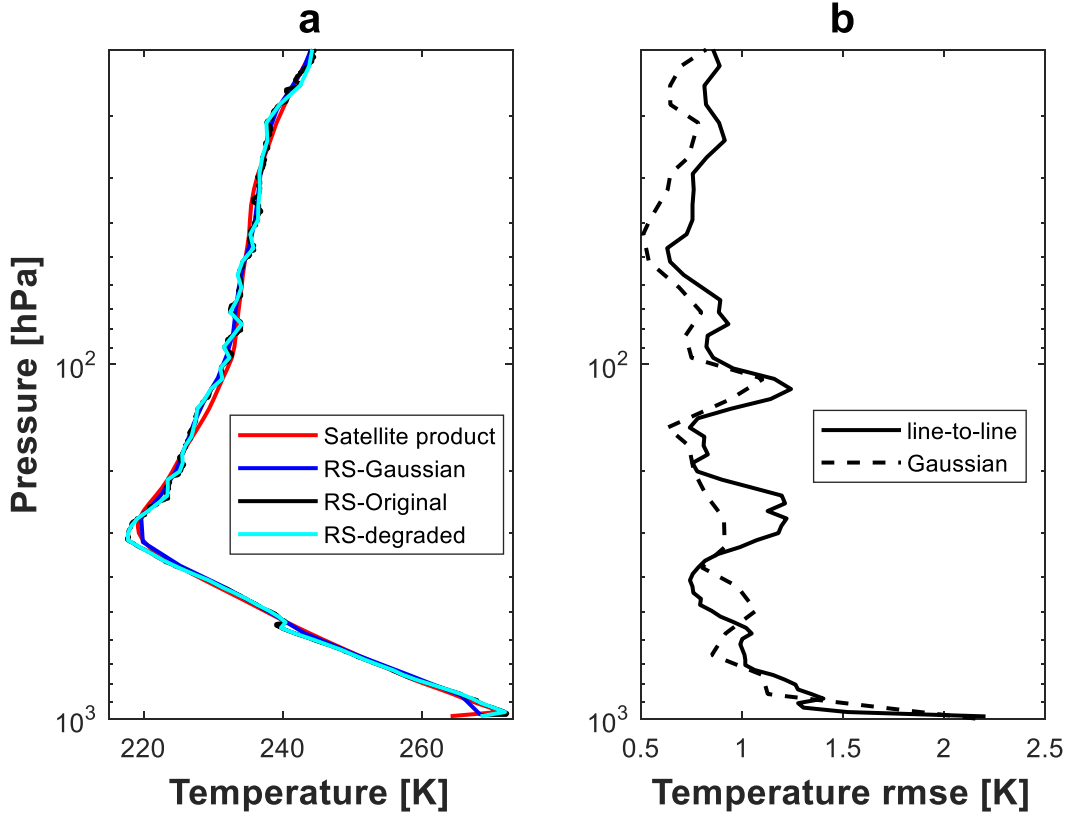


Figure 3.4: Exemplary profiles of temperature (a) and rmse (b) on the 10th of January, 2019. Radiosonde profiles are given on original resolution (black) smoothed to 1-km-resolution (blue) and degraded to the pressure grid of the satellites (cyan). The satellite profile is displayed (red) on the grid of the requested product. Profiles of temperature rmse are given for line-to-line (black) and for smoothed profiles (black, dashed).

3.2 Statistical metrics

Bias/Difference: The bias is defined as the average of the individual differences between satellite (S) and radiosonde (R) measurements at each of the M grid points (according to Wilks, 2006b).

$$bias = \frac{1}{M} \sum_{m=1}^M (S_m - R_m) \quad (5)$$

By this definition a positive bias indicates an overestimation of temperature by the satellite, while a negative bias is an indicator for an underestimation. The bias may lead to incorrect interpretations, for instance, positive and negative bias

values could cancel each other out when considering temporal and vertical averages.

In order to avoid this issue the root-mean-square-error (rmse) is introduced. Due to its mathematical definition the rmse (Wilks, 2006b) is always positive.

$$rmse = \sqrt{\frac{1}{M} \sum_{m=1}^M (S_m - R_m)^2} \quad (6)$$

Pearson-Correlation Coefficient (PCC):

A method to examine a dependency between two different mathematical or physical quantities is to calculate the Pearson-Correlation-Coefficient (PCC) (in accordance with Wilks, 2006a):

$$PCC = \frac{\sum_{i=1}^n [x_i - \bar{x}][y_i - \bar{y}]}{\sqrt{\sum_{i=1}^n [x_i - \bar{x}]^2} * \sqrt{\sum_{i=1}^n [y_i - \bar{y}]^2}} \quad (7)$$

In this equation x and y are the two different quantities at n samples, e.g. radiosonde and satellite measured temperatures and \bar{x}, \bar{y} their arithmetic mean.

The PCC is an indicator of a linear relationship between two variables. The PCC ranges from -1 to 1. Values close to -1 (perfect anti-correlation) and 1 (perfect correlation) indicate a strong linear dependency, whereas a PCC around zero suggest that there is no correlation between the variables (Wilks, 2006a).

4. Analysis of the temperature profiles

4.1 General comparison

Radiosonde and satellite temperature profiles are constructed according to section 3. Figure 4.1 shows the time-pressure evolution of temperature based on the pure radiosonde raw data from the surface up to roughly 30 km altitude. Several meteorological attributes of the atmosphere are recognized. First, the general structure of the polar summer atmosphere is captured having a warm troposphere and a relatively cold stratosphere. The temperature maximum is reached in the lowermost layers of the troposphere. Furthermore, the troposphere is characterized by variability of temperature due to passing storms and the development of temperature inversions in the boundary layer. Substantial temperature variations in the stratosphere are recognizable on weekly or seasonally scales. For instance, in beginning of the period (winter atmosphere regime), the dark blue colours extending over the low stratosphere indicate the last remnants of the Polar Vortex, which dissolves over the first two weeks. A slight and continuous stratospheric warming is recorded during the summer season. In addition a thermal tropopause has formed from mid-December onwards around the 250-300 hPa level (summer atmosphere). The data gaps (white space) of figure 4.1 are caused by early balloon bursts or missing radiosonde ascents in case of heavy storm events.

Figure 4.2 illustrates the time-pressure evolution of temperature build up from all collocated satellite overpasses. Hereby, temperature data is shown on the original vertical grid of the satellite products which consist of 76 predefined pressure levels from the surface up to 30 kilometres altitude. In figure 4.2 data gaps are displayed corresponding to time difference between the main synoptic standard time and the two surrounding overpasses of more than three hours. Obviously, in the satellite time series data gaps occur more frequently, particularly around 12 UTC (see also figure 2.2).

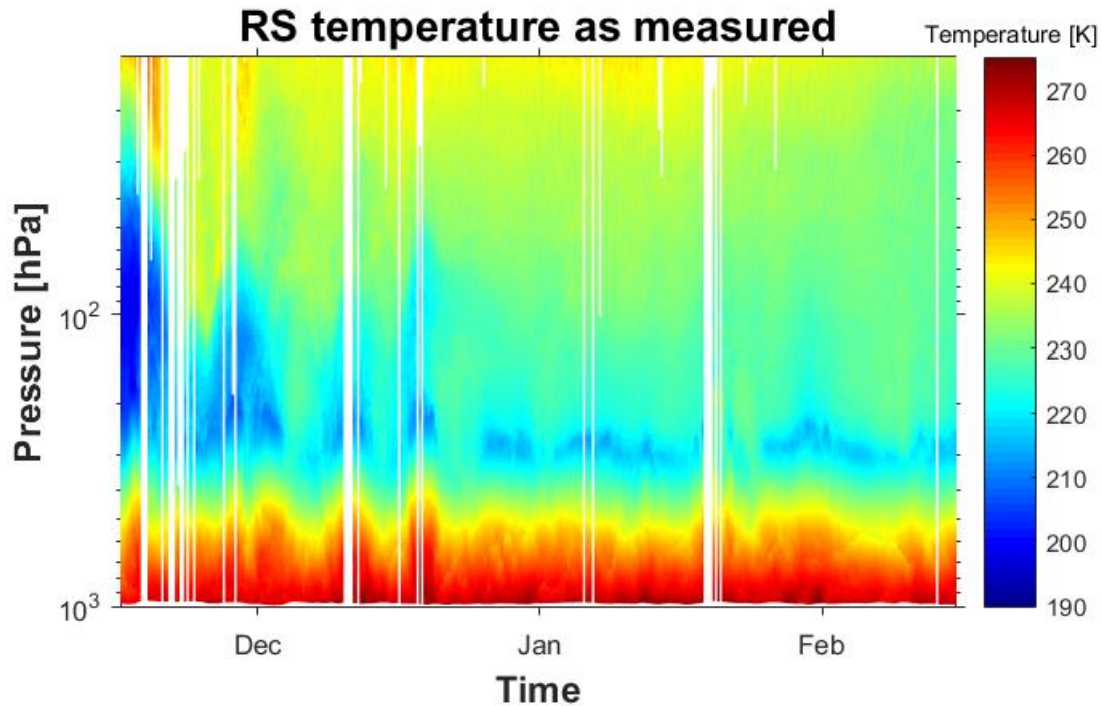


Figure 4.1: Time-pressure evolution of temperatures recorded by the radiosondes at original vertical sampling resolution. White space in between indicates missing ascents or early balloon bursts.

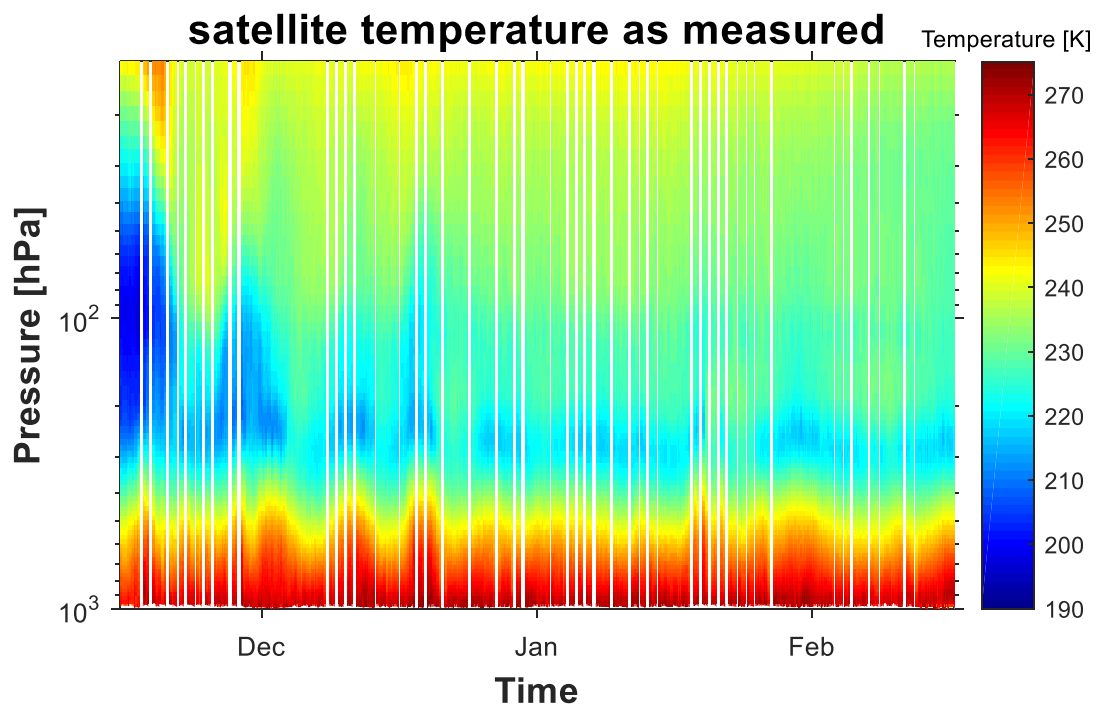


Figure 4.2: Time-pressure evolution of temperatures based on AIRS and IASI profiles at the pressure grid of the level 2 products. Data gaps (white space) are introduced, if the time difference between overpass and main synoptic standard time exceeds more than three hours.

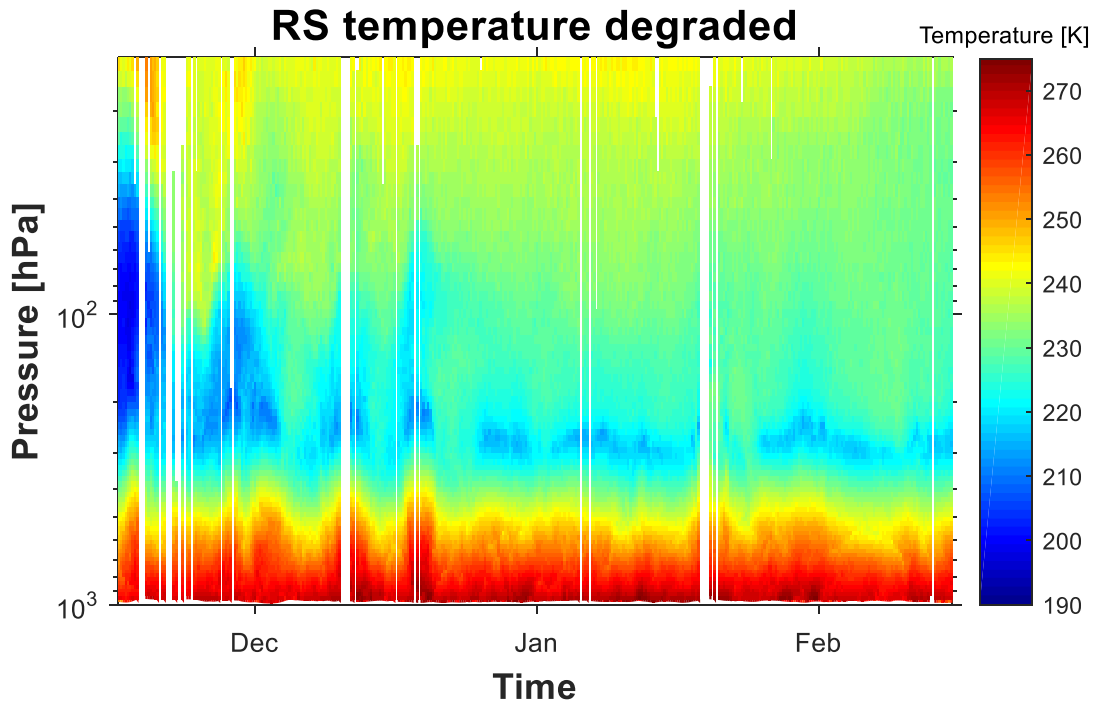


Figure 4.3: Time-pressure evolution of temperatures recorded by the radiosondes and interpolated at the pressure grid of the level 2 products. Data gaps (white space) are induced, corresponding to missing radiosonde launches or early bursts.

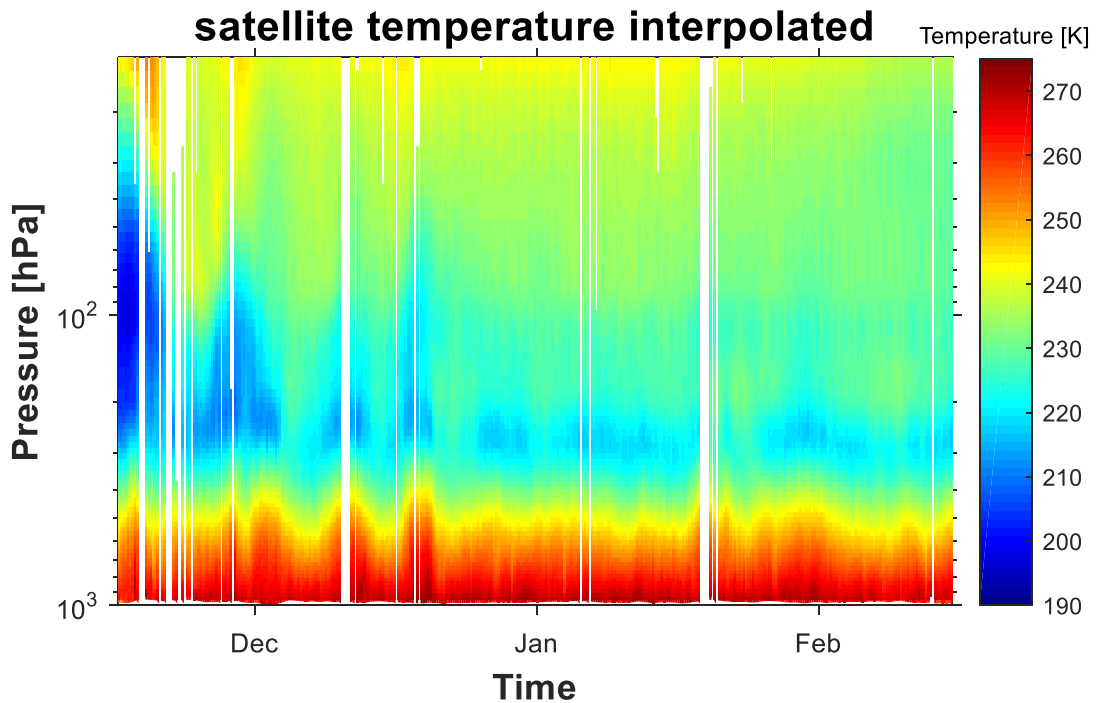


Figure 4.4: Time-pressure evolution of temporally interpolated IASI/AIRS temperature profiles at the pressure grid of the level 2 products. Data gaps (white space) are induced, corresponding to missing radiosonde launches or early bursts.

The original radiosonde temperature profiles are vertically degraded to the grid of the satellite products by interpolation on the 76 predefined levels (figure 4.3). The original satellite profiles are temporally interpolated according to the radiosonde ascent times (figure 4.4). It should be noted that missing satellite data is interpolated in time, independent of the length of the data gaps. Generally, with regard to the fundamental meteorological attributes, both illustrations (figure 4.3 and figure 4.4) show a high agreement. The general structure of troposphere and stratosphere is maintained by the satellite time series for the entire YOPP-SOP-SH. However, sharp temporal or vertical temperature contrasts, for example in the lower stratosphere or the lower troposphere (figure 4.3), appear to be more blurred and underestimated by the satellite time series (figure 4.4). Nevertheless, significant temperature differences between the two observational platforms can be worked out by applying the bias (section 3.2), which is an indicator of reliability of the satellite products (figure 4.5). Following the definition of the bias, bluish colours indicate an underestimation of atmospheric temperature by the satellites, while reddish colours implicate that satellites measure a higher temperature than the radiosondes. The key statements of figure 4.5 are that the temperature bias is predominantly about ± 1 K over wide parts of the profile and is smallest in the mid troposphere and in the stratosphere. However, over the entire vertical profile, the bias ranges between -8 and 8 K. The largest deviations occur in the lowermost troposphere and occasionally in other layers. At the tropopause level (~250-300 hPa) strong positive biases of approximately 4 K can be regularly observed from mid-December on. During the Polar Vortex regime in the beginning of the period, the temperature bias is mainly negative in the troposphere and positive in the stratosphere. Generally, none of the 76 vertical levels permanently exhibits positive or negative biases throughout the whole period, although between the 50-250 hPa interval, there appear to be bands of weak biases alternating between positive and negative values (± 1 K).

The time-pressure evolution showing the root-mean-square-error is provided in figure 4.6. In this context the rmse is equal to the absolute value of the bias. Hence, figure 4.6 underpins the main statements of figure 4.5. The rmse is slightly larger in troposphere than in stratosphere and reaches maximum mainly in the lowermost levels of the troposphere. Exceptionally large deviations occur in tropopause level and occasionally in the stratosphere (until January) and in troposphere for the entire period.

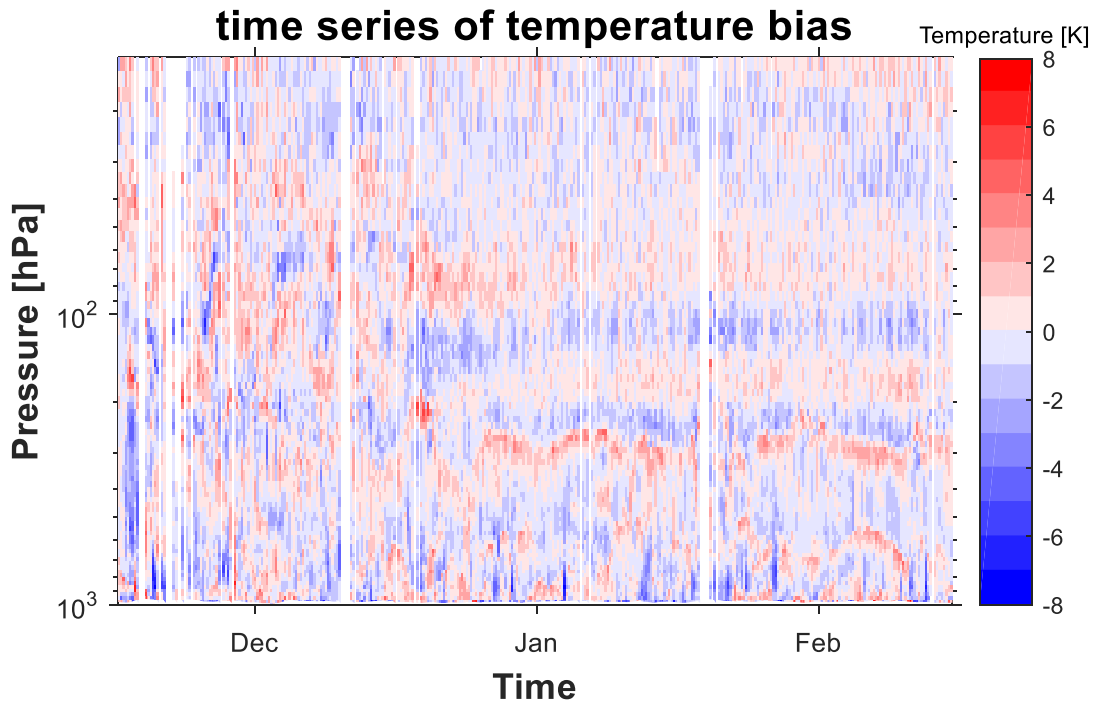


Figure 4.5: Time-pressure evolution of temperature bias (Sat-RS) at the pressure grid of the level 2 products and at radiosonde measurement times. Data gaps (white space) are induced, according to missing radiosonde launches or early bursts.

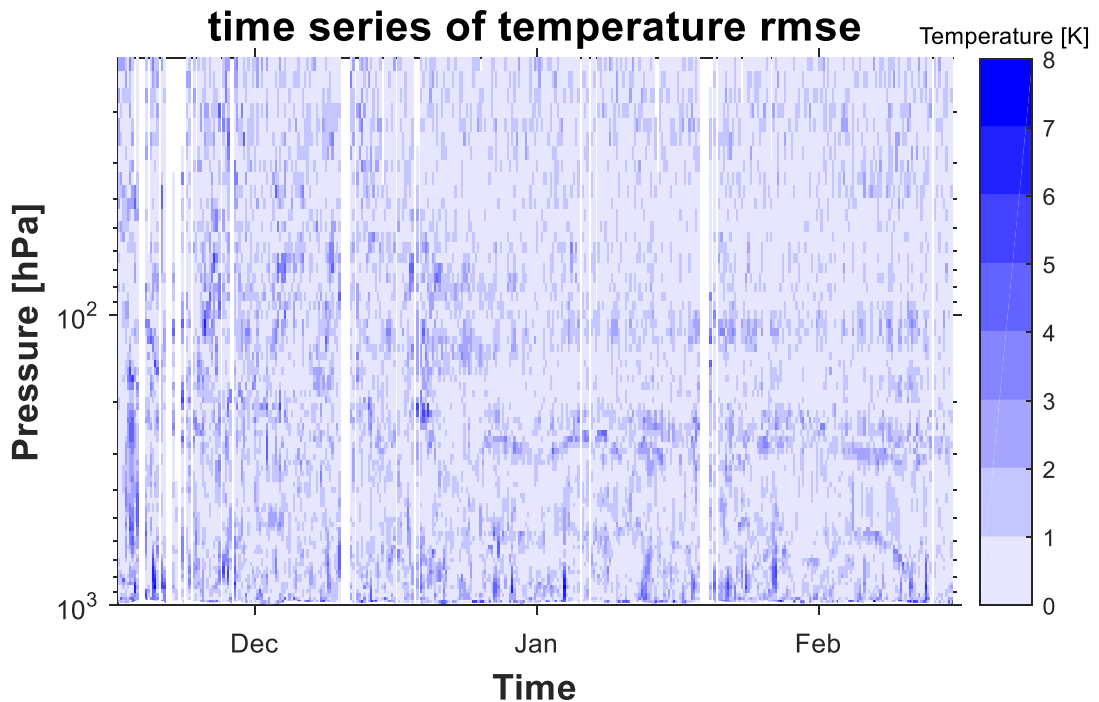


Figure 4.6: Time-pressure evolution of temperature rmse at the pressure grid of the level 2 products and at radiosonde measurement times. Data gaps (white space) are induced, according to missing radiosonde launches or early bursts.

Figure 4.7 contains profiles of temperature, bias and rmse averaged for the entire observing period. The temperature profiles (figure 4.7a) indicate that satellite and radiosondes particularly coincide up to the tropopause (~300 hPa) within one degree. The temperature minimum at the tropopause base is well-captured. On average, deviations are around 1 K in troposphere and slightly lower than 1 K in stratosphere. Local maxima of rmse occur near surface (more than 2 K) and in tropopause as well as around the 100 hPa level at which the rmse is about 1.5 K (figure 4.7c). The largest negative biases appear at the surface level as (figure 4.7b) as well as just below the 100 hPa level, whereas in tropopause a positive bias can be worked out. The profile of bias shows a zig-zag-shape between 70 to 300 hPa where positive and negative deviations are displayed.

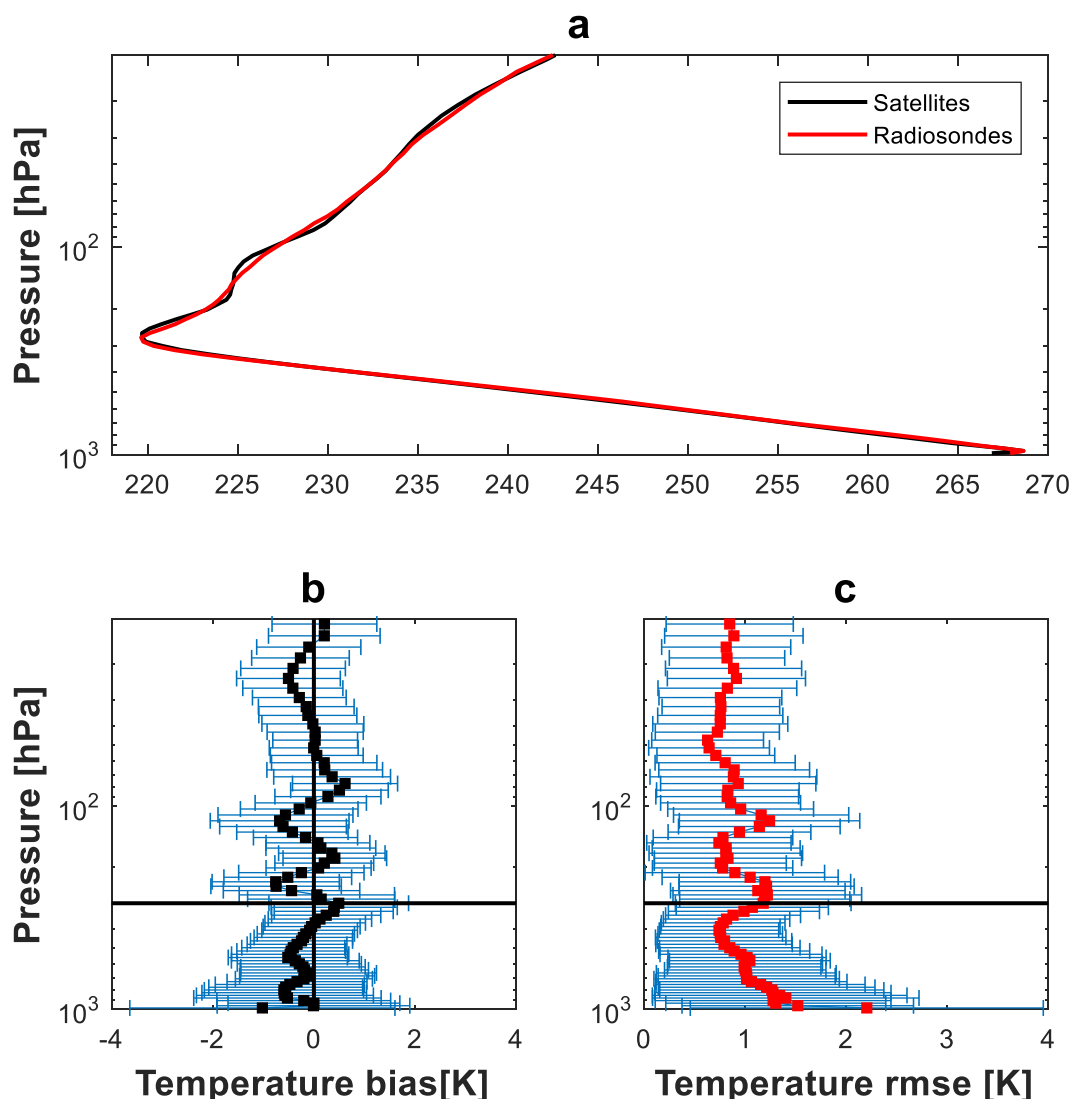


Figure 4.7: Profiles of temperature (a), bias (b) and rmse (c) averaged for the entire YOPP-SOP-SH. The blue error bars display the standard deviation, while the horizontal black lines indicate the mean tropopause level.

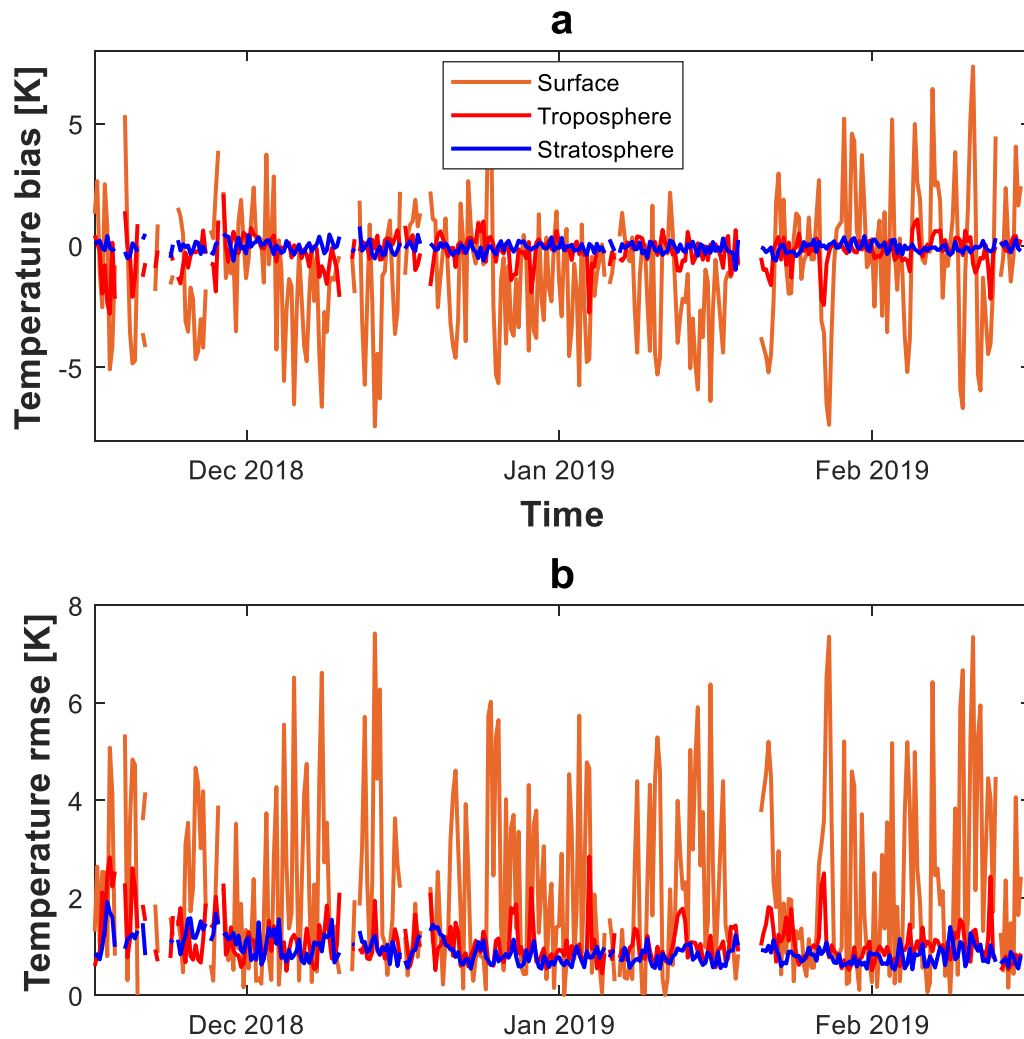


Figure 4.8: Time series of temperature bias (a) and rmse (b) for different vertical layers, the surface (brown), the troposphere (red) and the stratosphere (blue).

Temperature deviations are computed for the full profile and for particular layers regarding bias (figure 4.8a) and rmse (figure 4.8b). Particularly, the surface exhibits the largest deviations increasing up to 8 K. In most cases there is a strong negative bias at the surface indicating that the satellite products underestimate the surface temperature. In general, rmses are marginally larger in the troposphere (1.06 K) than in the stratosphere (0.90 K). Table 4.1 presents rmse and bias averaged for the different main synoptic times and for different atmospheric layers. The overall rmse for the season is 0.97 K with a very week diurnal variation of 0.11 K. Rmse is maximum at the surface level (1.39-2.57 K) and better in stratosphere (0.88-0.96 K) than in troposphere (0.97-1.12 K). In the troposphere rmse are at largest at 00 and 18 UTC, while at the surface rmse are at largest at 00 and 06 UTC. Temperature biases are small, for the full time

series about -0.14 K. Biases are mainly negative, except in the stratosphere at 06 UTC. In the troposphere diurnal variations of bias are smaller than rmse variations as positive and negative deviations cancel each other out. In the stratosphere, diurnally fluctuations of bias are larger than rmse variations.

Table 4.1: Average of rmse (bias) for the synoptic standard times and the entire period.

	Entire Profile	Surface	Troposphere	Stratosphere
Total	0.97 (-0.14) K	1.90 (-1.03) K	1.06 (-0.22) K	0.90 (-0.07) K
00 UTC	0.99 (-0.11) K	2.57 (-1.23) K	1.11 (-0.22) K	0.88 (-0.03) K
06 UTC	0.95 (-0.07) K	1.99 (-0.17) K	1.04 (-0.28) K	0.88 (0.08) K
12 UTC	0.92 (-0.21) K	1.39 (-1.18) K	0.97 (-0.23) K	0.88 (-0.20) K
18 UTC	1.03 (-0.15) K	1.60 (-1.55) K	1.12 (-0.16) K	0.96 (-0.15) K

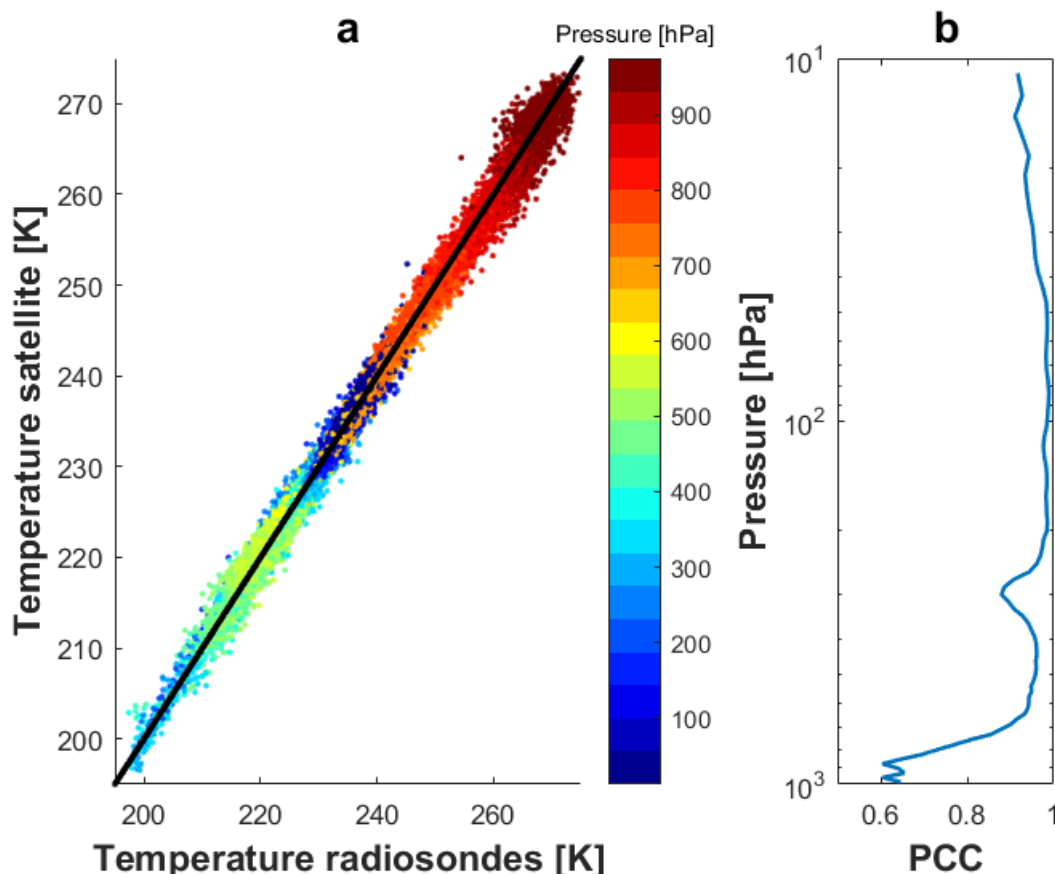


Figure 4.9: Scatter plot of radiosonde and satellite temperatures coloured by their altitude (a) and the corresponding vertical profile of the PCC averaged for the YOPP-SOP-SH (b).

A potential height relationship between radiosonde and satellite profiles is examined in figure 4.9 showing a scatter plot in which different marker colours highlight measured temperatures at different height levels (figure 4.9a). Figure

4.9b contains a vertical profile of the Pearson-correlation-coefficient averaged for the entire measuring period. Both, the clear diagonal shape of the scatter plot as well as the PCC profile indicate a strong relation between radiosonde and satellite temperatures. The PCC is larger than 0.9 for wide parts of the profile, particularly in middle-troposphere and above the tropopause level. At the tropopause level the PCC reaches a local minimum of about 0.85. In the lowermost troposphere, the correlation of the different measurements is only around 0.6 and 0.65. A similar effect is recognizable in figure 4.9a, where the diagonal widens to some extent underneath the 700 hPa level.

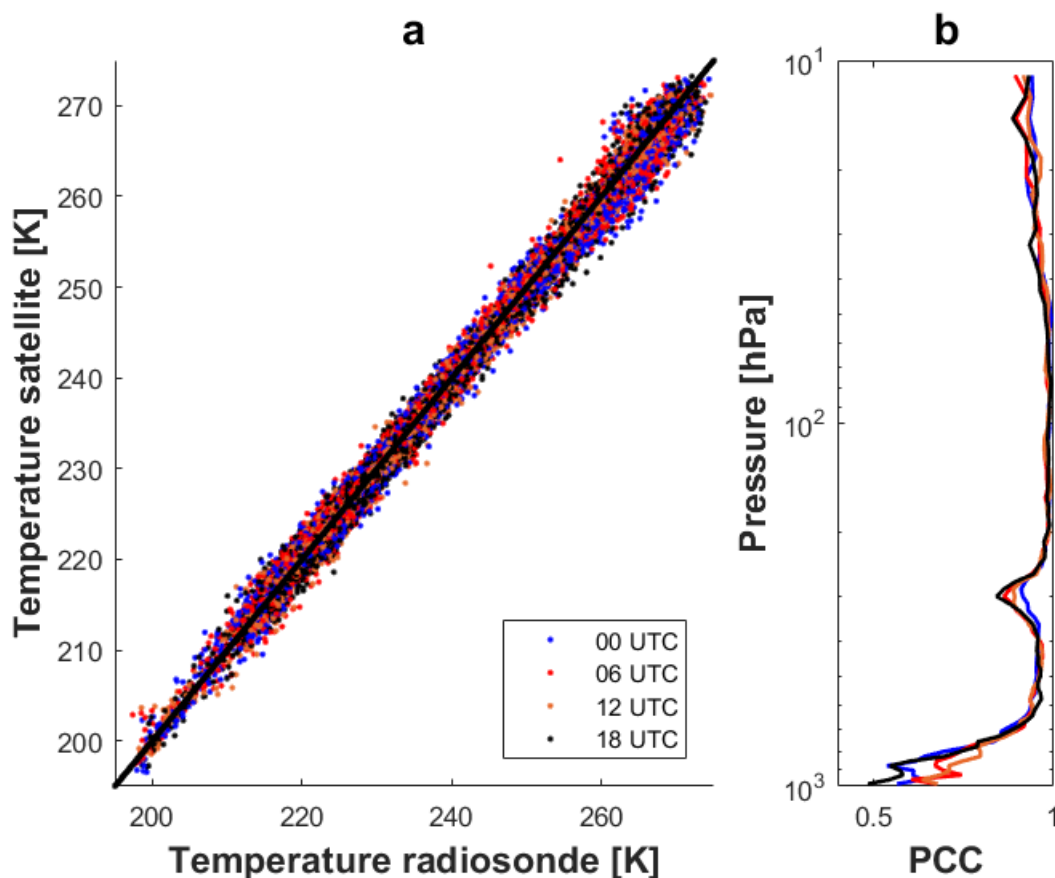


Figure 4.10: Scatter plot of radiosonde and satellite temperatures for the four main synoptic times 00 UTC (blue), 06 UTC (red), 12 UTC (brown) and 18 UTC (black) (a) and their corresponding vertical profile of the PCC (b).

Diurnal correlations are investigated in figure 4.10 illustrating the relations between the recorded temperatures separately at the four main synoptic times. The markers appear to be randomly arranged on the diagonal, so is no clear diurnal dependency detectable (figure 4.10a). In addition, the vertical PCC exhibits a similar shape for all main synoptic time, although the curves differ in the lowermost part of the profile (figure 4.10b). At the surface level the PCC ranges from roughly 0.5 (18 UTC) up to 0.7 (06 and 12 UTC).

4.2 Comparison of AIRS and IASI

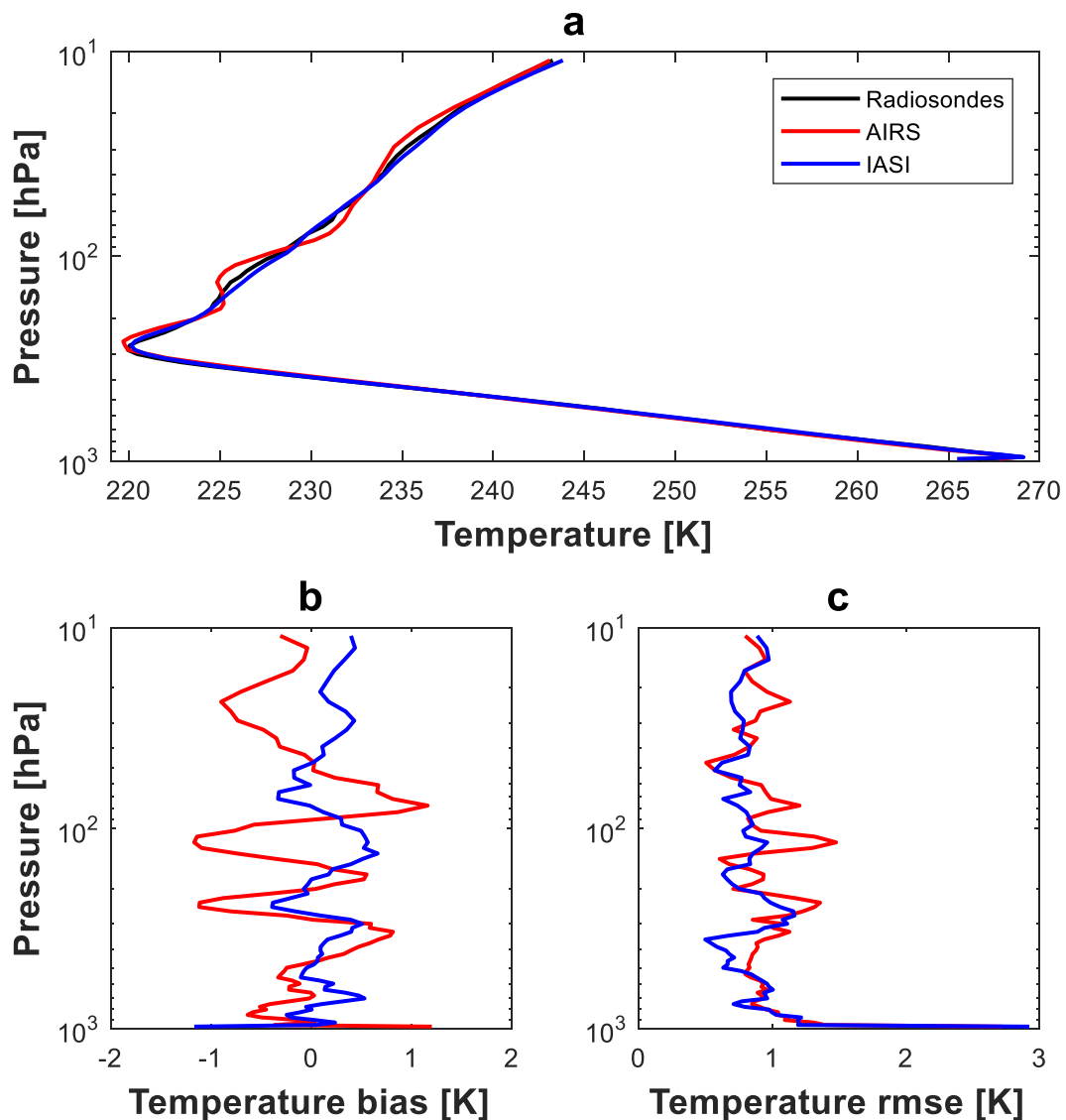


Figure 4.11: Separate analysis of IASI and AIRS temperature products concerning full profile (a), bias (b) and rmse (c) averaged for observations at 00 UTC.

AIRS and IASI do frequently provide temperature profiles around the 00 UTC radiosounding. Thus, a separate assessment of AIRS' and IASI's products is done by comparing profiles (figure 4.11) at this time. We perform a comparison exclusively, if a particular radiosounding is concurrently matched by both sounders. This criterion applies to 58 profiles at 00 UTC. In the troposphere, the mean temperature profiles indicate that AIRS and IASI show a very high agreement with each other and with respect to the radiosonde observations (figure 4.11a). The profiles of rmse also show that the overall accuracy of the two sounder is of same order, although IASI is slightly better at nearly all pressure

levels (figure 4.11c). However, substantial differences are visible in the stratosphere, where the derived satellite products considerably distinguish from the radiosounding. Especially AIRS' temperature product displays strong systematically variations of bias extending from the upper troposphere up to 25 hPa (figure 4.11b). IASI also shows larger biases at these levels, but its deviations are significantly lower. It is furthermore noticeable, that AIRS' strong positive bias corresponds to a local minimum of IASI's bias at 50 hPa. On the contrary, the negative bias of AIRS around 100 hPa corresponds to a strong positive bias of IASI. Further differences occur at the surface level even though the rmse is of similar order. On average AIRS produces a positive bias of more than 1 K at the surface, whereas IASI shows a strong negative bias of more than 1 K at 00 UTC.

4.3 Temporal mismatch

Typically, satellite overpass times and radiosonde measurements do not correspond in time. Time differences between radiosondes and matched satellite profiles vary during YOPP-SOP-SH and constitute a potential error source, called "temporal mismatching". The temporal mismatch is individual for each measurement and can vary between nearly zero and five hours (figure 4.12). Figure 4.12 highlights the temporal differences between the closest collocated satellite profile and the radiosonde launch time at the four synoptic standard times. The time differences are predominantly less than two hours at 00 and 18 UTC. On the contrary, temporal mismatch is more variable at 06 and 12 UTC increasing regularly up to four hours.

Figure 4.13a highlights the relationship between temporal mismatch and rmse. Due to the seemingly random dispersion, it can be seen that both time series are not significantly correlated (PCC = 0.14). Corresponding to figure 4.13a large rmse occur independently from the magnitude of time differences between radiosondes and satellite overpass. Figure 4.13b shows profiles of rmse averaged for four regular bins of temporal mismatches. The red curve for instance, displays the computed rmse for all profiles with a temporal mismatch of more than 2.8 hours. The red curve stands out from the others only marginally in the troposphere and around the 100 hPa level. An increase of the temperature rmse with increasing time offset between radiosondes and satellites cannot be proven.

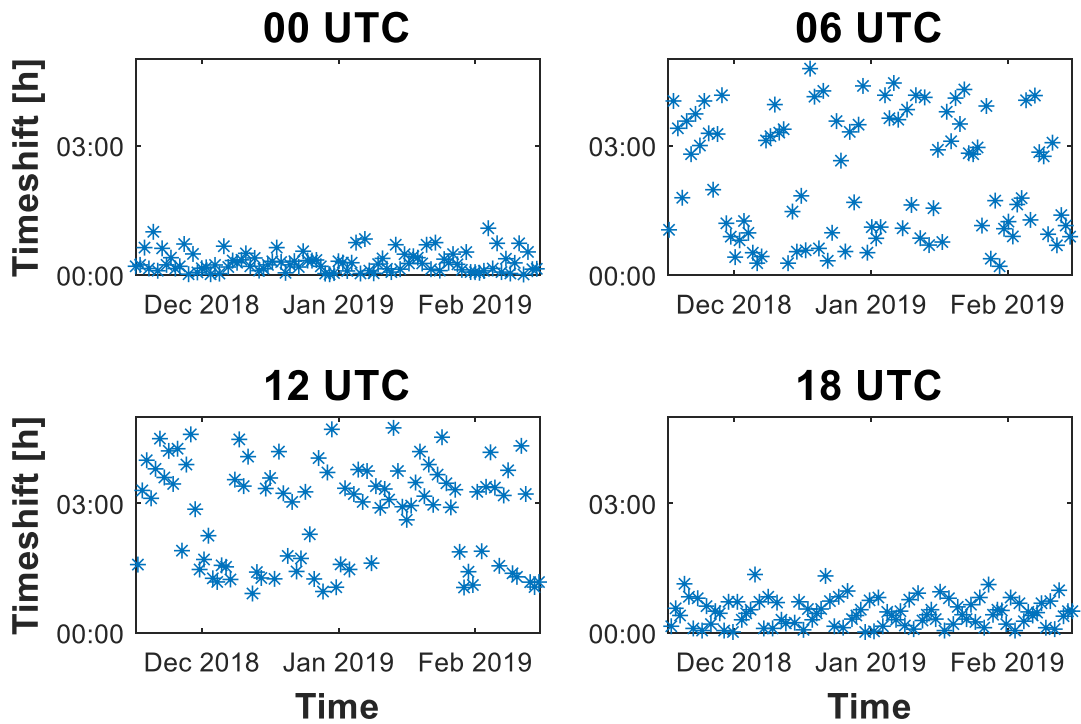


Figure 4.12: Temporal mismatch. Time difference between nearest collocated overpass and launch time separated for the synoptic standard times.

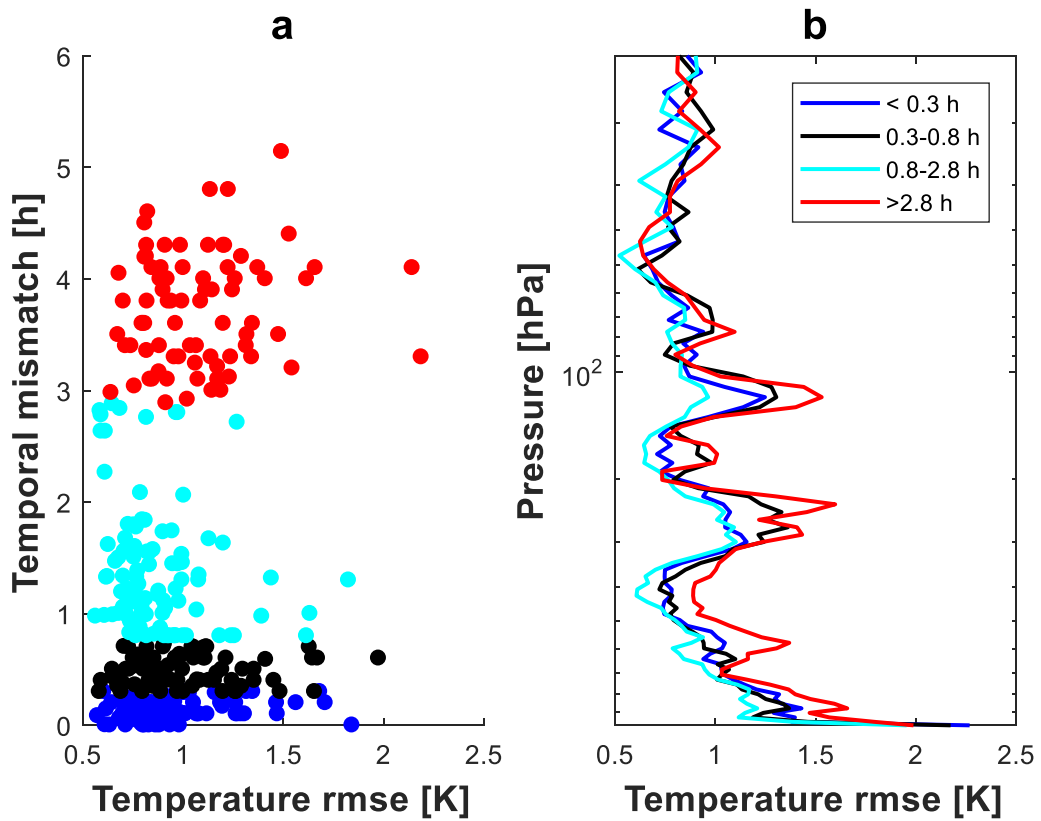


Figure 4.13: Scatter plot of rmse and temporal mismatch (a) and profile of rmse averaged for different bins of temporal mismatch (b).

4.4 Horizontal mismatch

Another source of deviations of the measured temperatures could be horizontal mismatching, which is defined as the horizontal distance of the collocated IFOV centre and the mean geographical position of the radiosonde during its ascent. Although only IFOV's are collocated within a 50 km circle around Neumayer Station the distance to the sonde may exceed this value due to the horizontal displacement of the sonde. The relation of horizontal mismatch and temperature rmse is displayed in figure 4.14 containing a scatter plot of the horizontal mismatching (figure 4.14a) and profiles of rmse, computed for different bins of mismatching (figure 4.14b). The correlation between the distance of IFOV centre to the radiosonde and the rmse is still poor ($PCC = 0.15$). The rmses do not inevitably rise for larger horizontal mismatches as they occur independently from the magnitude of mismatch (figure 14a). On the other hand, the largest horizontal mismatch (figure 4.14b, blue curve) shows the largest rmse at nearly all altitudes. Especially, the tropospheric's rmse is occasionally 0.5 K larger, compared to smaller horizontal mismatches (e.g. red curve).

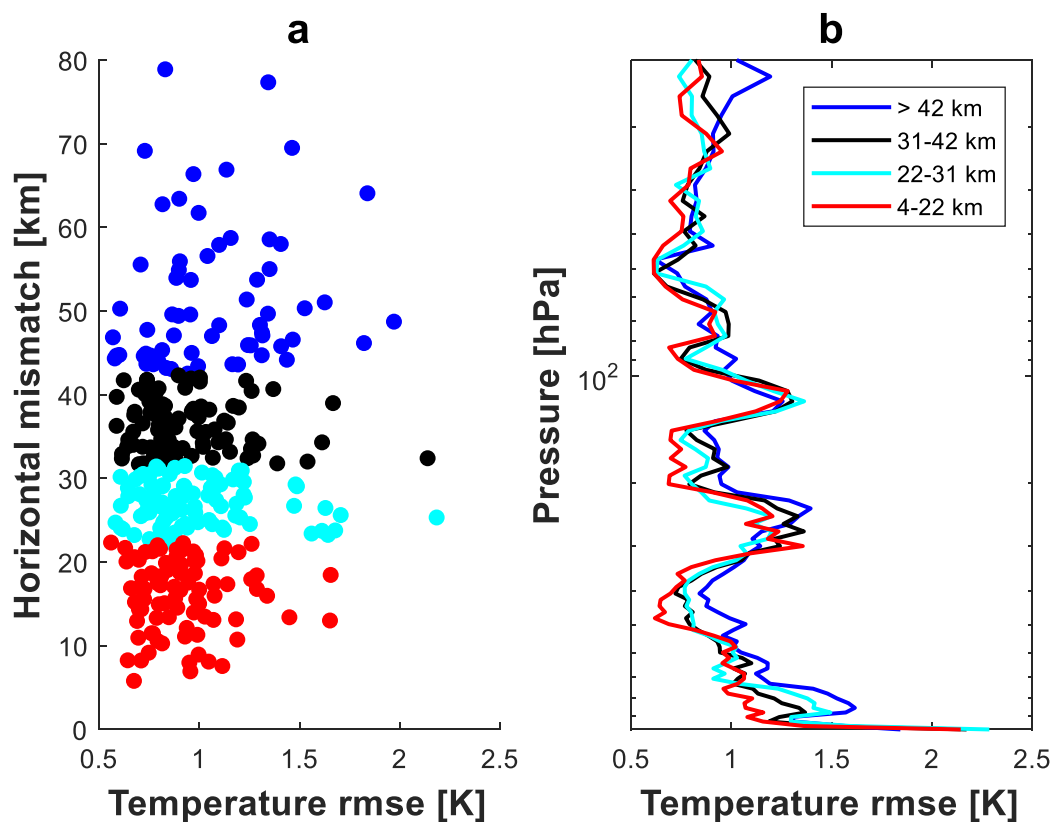


Figure 4.14: Scatter plot of rmse and horizontal mismatch (a) and profile of rmse averaged for different bins of horizontal mismatch (b).

4.5 Impact of cloud cover

Table 4.2: Categories of cloudiness: Classification and number of occurrence.

Category	Clear sky	CC Low	CC High	Overcast	Snowfall
Cloud Coverage	0/8	1/8 to 4/8	4/8 to 7/8	8/8	Snowfall
Number of observation	19	84	99	89	48

Since IR satellite measurements are sensitive to cloud, reliability of the satellite derived time series could depend on cloudiness. In order to assess the influence of clouds, the entire measuring period is divided into specific categories of cloudiness, namely “Clear sky”, “Low cloud coverage”, “High cloud coverage”, “Overcast” and “Snowfall”. Number and classifications of the categories can be found in table 4.2. The categories are determined by visual synoptic observations which are made directly after the radiosonde launch (table 4.2). Rmses and biases are provided for the different categories of cloudiness and for different atmospheric layers (table 4.3, figure 4.15 and figure 4.16).

Corresponding to the entire profile (figure 4.15 and figure 4.16, red markers), the rmse increases with increasing cloud coverage while the bias tends to become more negative. However, these effects are most significant in the troposphere (blue markers) in which the bias falls from 0.09 K (clear sky) to -0.59 K (snow) whereas the rmse increases about 0.4 K. In the stratosphere variations of biases are weak in terms of cloudiness (-0.14 to 0.01 K). Furthermore, clear sky profiles display a larger rmse than partly clouded scenes in the stratosphere. In principle, clear sky profiles as well slightly clouded profiles are of comparable accuracy in the troposphere. At the surface (black markers) deviations also tend to be larger for increasing cloud coverage except for clearsky profiles which show the strongest bias (-0.50 K) and a remarkable large rmse (1.63 K). Cloudless profiles excluded, at the surface the rmse rises with increasing cloudiness by 0.60 K while bias falls by 0.7 K.

Table 4.3: Rmse (bias) averaged for the categories of cloudiness and for the different atmospheric layers.

	Entire Profile	Surface	Troposphere	Stratosphere
Clearsky	0.92 (0.06) K	1.63 (-0.50) K	0.83 (0.09) K	0.95 (0.01) K
CC Low	0.84 (0.02) K	1.24 (0.33) K	0.81 (0.01) K	0.83 (0.01) K
CC High	0.92 (-0.11) K	1.39 (-0.06) K	0.99 (-0.07) K	0.84 (-0.13) K
Overcast	1.08 (-0.24) K	1.65 (-0.03) K	1.21 (-0.39) K	0.96 (-0.11) K
Snow	1.12 (-0.35) K	1.84 (-0.37) K	1.23 (-0.59) K	1.02 (-0.14) K

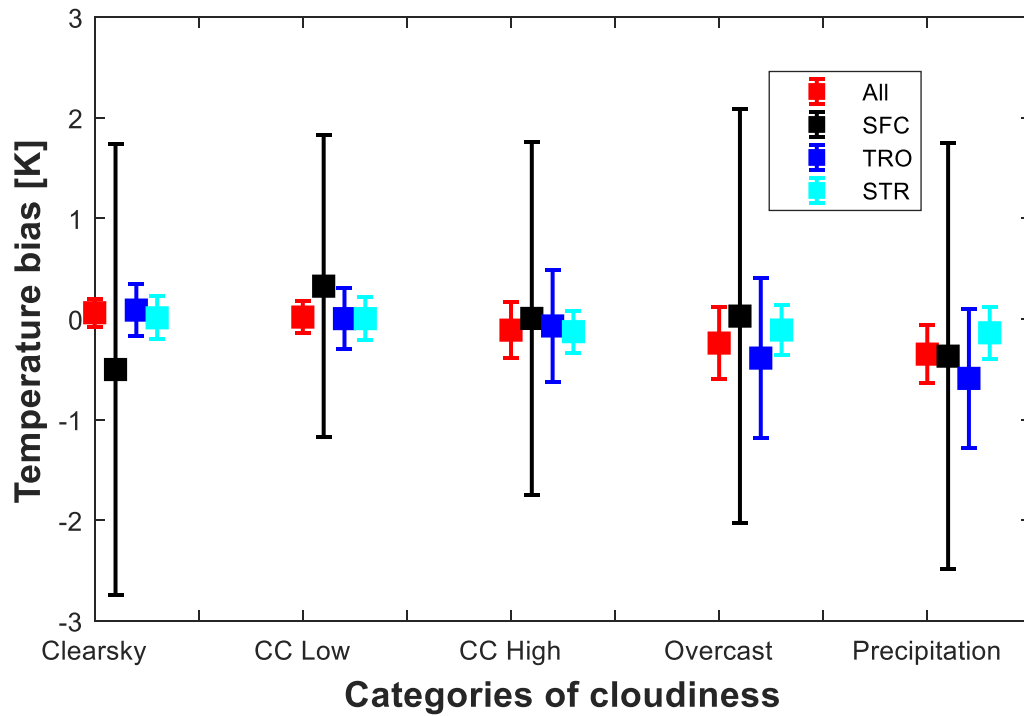


Figure 4.15: Temperature bias and its standard deviation averaged for the categories of cloudiness and for different altitude levels (red: entire profile, black: surface, blue: troposphere and cyan: stratosphere).

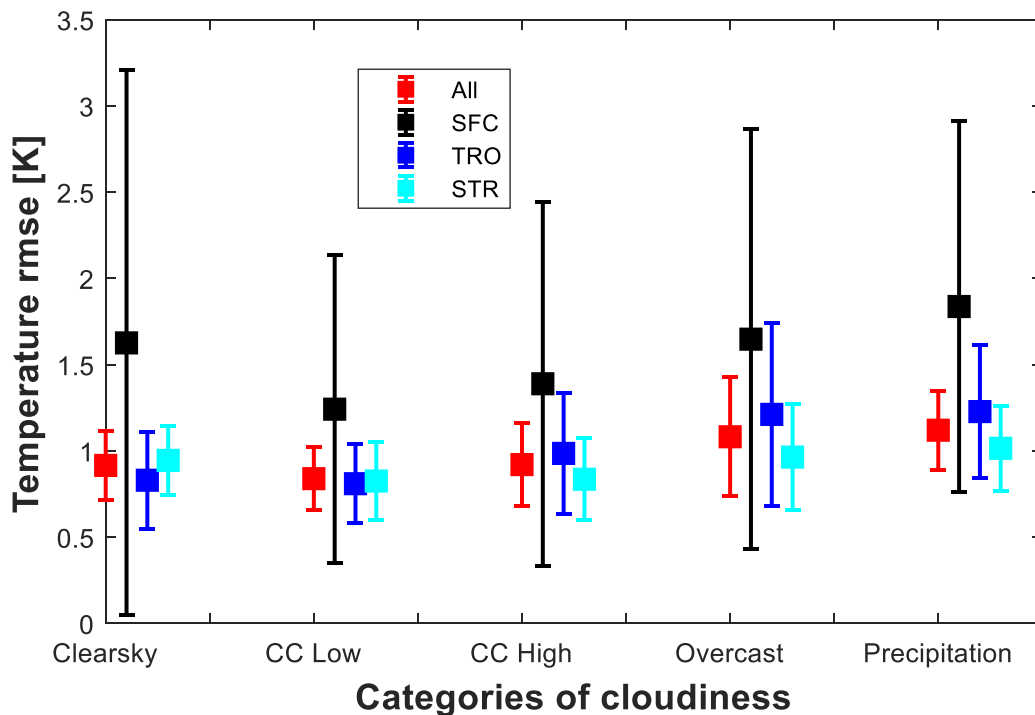


Figure 4.16: Temperature rmse and its standard deviation averaged for the five different categories of cloudiness and for different altitude levels (red: entire profile, black: surface, blue: troposphere and cyan: stratosphere).

4.6 Surface-based temperature inversions

Typically, the largest deviations between radiosonde and satellite-based temperature profiles occur in the lowermost troposphere. This layer is dominated by a diurnal cycle of formation and regeneration of surface-based temperature inversions. SBTIs are characterized by different attributes such as frequency of occurrence and intensity (table 4.4 and table 4.5). A temperature inversion is detected, if the temperature increases from the surface level to the adjacent level above it. The temperature difference of the recorded maximum and surface air temperature defines the intensity of a SBTI. In the detection algorithm also weak and flat inversion layers are allowed, since no thresholds are set in terms of vertical extension of the inversion or intensity. The full resolved radiosonde measurements are assumed to be close to the true physical state of the atmosphere. This enables to analyse to what extent attributes of the surface-based temperature inversions can be captured by the satellite products at Neumayer Station. Table 4.4 and table 4.5 display the detected attributes of SBTI measured by the radiosondes and satellites.

Table 4.4: Attributes of SBTIs detected by the radiosondes.

	Number	Frequency	Intensity
Total	160 of 339	47.20 %	3.92 K
00 UTC	50 of 87	57.47 %	4.45 K
06 UTC	64 of 82	78.04 %	4.50 K
12 UTC	27 of 85	31.76 %	3.02 K
18 UTC	19 of 85	22.35 %	1.86 K

Table 4.5: Attributes of SBTIs detected by the satellite products.

	Number	Frequency	Intensity
Total	228 of 339	67.26 %	3.17 K
00 UTC	71 of 87	81.61 %	3.61 K
06 UTC	67 of 82	81.71 %	3.73 K
12 UTC	54 of 85	63.53 %	2.01 K
18 UTC	36 of 85	42.35 %	2.96 K

Although the weather at Neumayer Station during austral summer is characterized by regularly passing storms alternating with anticyclones, a clear diurnal cycle of temperature inversions (table 4.4) is recorded by the radiosondes. Most inversions are captured at 00 (and 06 UTC) by roughly 57 (78) % of all measurements, while the frequency of observed inversions

decreases to about 32 % at 12 UTC, respectively 22 % at 18 UTC. The satellite profiles do also provide a diurnal cycle, however, frequency of temperature inversions is overestimated at all observation times (table 4.5). Furthermore, the frequency of detected SBTI's reaches is similar for 00 and 06 UTC (~82 %). At 12 and 18 UTC the number of inversions recorded by the satellites is roughly twice as much compared to the radiosonde records.

Corresponding to the diurnal cycle of frequency of occurrence, the intensity of temperature inversions also shows daily variations. Strongest inversions are observed by radiosondes at 00 and 06 UTC with an intensity of roughly 4.5 K while inversions tend to be weaker at 12 (~3 K) and 18 UTC (about 1.9 K). The satellite derived profiles indicate a similar cycle, although the intensity on average is underestimated by approximately 1 K at 00, 06 and 12 UTC. On the contrary, the intensity is clearly overestimated (~1 K) by the satellites at 18 UTC.

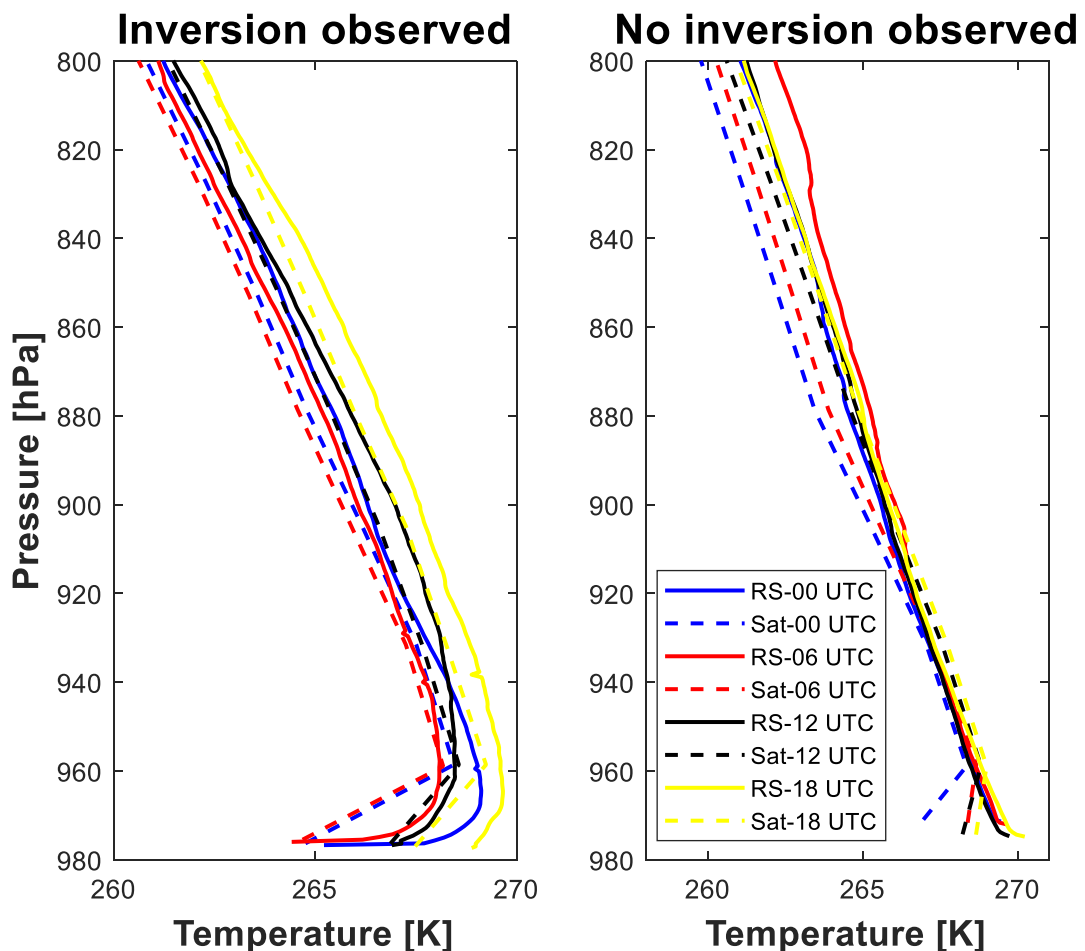


Figure 4.17: Temperature profiles of the lowermost troposphere: 1. Temperature inversion is observed by the radiosondes and 2. No temperature inversion is detected by the radiosondes. Profiles are averaged in accordance with the observed state.

The overestimation of SBTIs by satellites is highlighted in figure 4.17 which contains the mean temperature profiles depending on whether an inversion is observed by the radiosondings (figure 4.17a) or not (figure 4.17b). If an inversion is observed, the mean temperature profile of the satellites also shows an inversion of similar intensity at all times. If the radiosondes do not observe inversions, the satellites reproduce on average a weak surface-based inversion throughout the day, related to an underestimation of surface temperature.

5. Discussion

The radiosonde data and assimilated satellite profiles recorded during the campaign YOPP-SOP-SH are used to generate time series of temperature profiles (section 4) extending over the entire polar summer period. Comparison of these time series enables us to assess the accuracy of AIRS- and IASI-based temperature profiles at Neumayer Station, Antarctica. Recent studies found that deviations of satellite products in the Antarctic vary for different locations (e.g. Boylan et al., 2016). However, they provide accuracies averaged for wide areas only. This analysis evaluates the performance of the AIRS and IASI products for a large period and at one specific location. First, we investigate in which layers of the atmosphere and at which time of the day the largest deviations typically occur (section 4.1). The following sections provide explanations for exceptionally large deviations. Potential error sources are investigated and quantified in terms of differences between AIRS and IASI, temporal and horizontal mismatch, impact of cloud cover and regarding surface-based temperature inversions (sections 4.2-4.6).

General assessment

Fundamentally, the satellite-derived products are able to reproduce important meteorological attributes of the (polar) atmosphere, such as the Polar Vortex, temperature inversions, the tropopause layer, seasonal trends and minor warming events (figure 4.1-4.4). On the other hand, due to the limited vertical resolution of the satellite sounders these attributes are often systematically blurredly represented and underestimated in intensity. The comparison shows that the total rmse of the temperature time series is about 0.97 K and shows a small negative bias of -0.14 K. For wide parts of troposphere and stratosphere therefore, the satellite-derived products meets the 1 K/1 km demand of NWP. It has to be note, that the observing period can be divided into different major regimes (summer and winter atmosphere). Since the winter regime is only

present in the first few days, all results are only representative for the summer atmosphere. However, figure 4.5 indicates that distribution of positive and negative biases is substantially different for the two regimes.

The time-pressure evolution of bias and rmse shows that deviations are generally weak in the middle troposphere and in stratosphere (rmse of roughly 0.5 K). On average, the bias in troposphere is negative (0.5-1 K, figure 4.7) which confirms the cool bias found in Boylan (2016). The precision of the satellite profiles decreases in the lowermost troposphere and at the tropopause level (250-300 hPa). Both layers are characterized by a reversal of vertical temperature gradient as part of temperature inversions or at tropopause base. These meteorological structures are of limited vertical extent, typically about several 100 metres. Since the vertical resolution of the IR sounders is approximately 1 km, SBTI and tropopause level cannot be resolved accurately. As a consequence, temperatures around the tropopause level are systematically overestimated by the sounder products (up to 4 K), while temperatures in the lowermost troposphere tend to be underestimated by several degrees. Furthermore, in the lower stratosphere the constructed satellite profiles continuously displays bands of weak positive (150-250 hPa, 50-90 hPa) and negative biases (100-150 hPa and immediately above tropopause level) from mid-December onwards (summer atmosphere). The temperature in the stratosphere typically rises continuously and slowly with increasing altitude. For this reason, the limited vertical resolution of the satellites cannot be the key explanation for the homogeneously occurring deviations in the lower stratosphere. Instead, a separate comparison of the two different sounder products shows that deviations in the stratosphere are mainly caused by the systematic errors of the AIRS product. AIRS produces large negative biases of about 1 K at around 250 hPa and at 100 hPa altitude and strong positive biases at 50-90 hPa (1 K) and around the 200 hPa (0.5 K) level (figure 4.12). Both, altitude and magnitude of the deviations of the AIRS-only product are consistent with past studies (e.g. Dang et al., 2017). AIRS' deviations correspond to bands of positive and negative biases which are found around these levels. Due to the temporal interpolation, the AIRS profiles provide a significant contribution to the reconstructed profiles, notably on days when IASI data is not available. Conclusively, the AIRS product reduces the quality of the satellite data especially in the stratosphere, where the bias of AIRS is predominant. Diurnal variations of errors in general could be caused through temperature variations or due to a variable availability of satellite data. The daily number of AQUA, Metop-A and Metop-B measurement can vary between 2 and 14 per day at Neumayer Station. Satellite overpasses and therefore data gaps occur at certain time intervals at each day (figure 2.2). Results indicate that the temperature rmse shows a weak diurnal cycle only of about 0.11 K with largest

rmse at 18 UTC (1.03 K) and lowest at 12 UTC (0.92 K) (table 4.1). This implicates that the existing data gaps (e.g. at 12 UTC) can be widely compensated by the temporal interpolation, since the accuracy is of same magnitude for all synoptic standard times. The usage of three atmospheric sounders seems to be sufficient to obtain temperature information of similar accuracy throughout a day at Neumayer Station.

In spite rmse and bias do not display significant diurnal variations with respect to the entire profile (figure 4.11) differences can be recognized at the surface level. Generally, satellite and radiosonde temperatures are highly correlated (PCC > 0.9) particularly in the middle-troposphere and in stratosphere (figure 4.10). Correlations are slightly weaker at the tropopause level (PCC ~ 0.85) and weak below 700 hPa (PCC ~ 0.65) with minimum at the surface. Deviations of the stratosphere and troposphere are of similar order (~1 K) except for the tropopause and at the surface. Differences reach their maximum value either at the surface or within the lowermost levels of the troposphere and can increase up to ± 8 K. Substantial diurnal variations are exclusively detected at the surface level at which bias and rmse on average show variations of more than 1.5 K (table 4.1) extending from 1.39 K at 12 UTC to 2.57 K at 00 UTC. On average, deviations of surface air temperatures are twice as high as in the rest of the profile and predominantly negative. The wide range of deviations at the surface may be explained by two issues. On the one hand, particularly the surface level is characterized by high daily variability at Neumayer Station e.g. as part of the SBTI formation cycle (section 1). Satellite overpass and radiosonde launch do not accurately coincide in time, so small temporal mismatches could lead to large temperature differences at the surface. According to this statement, biases at 06 and 18 UTC should be positive, since the collocated overpasses are closer to the maximum of sun's position than the radiosondes. However, biases are also negative at these times, so temporal mismatching alone does not provide a reasonable explanation for diurnal variations of rmse/bias at the surface. On the other hand, the derived surface temperature products of AIRS and IASI are fundamentally different. IASI's surface product is retrieved separately by a surface retrieval and contains the surface skin temperature, which is the soil temperature. As the radiosondes records consist of the 2-meter air temperature, the IASI's surface skin temperature should be typically lower than the surface temperature of the radiosonde profile. The AIRS product contains the surface air temperature which is based on an extrapolation of the retrieved profile to the surface pressure (section 2.1). The surface pressure is overestimated by several hectopascals, so AIRS' derived surface air temperatures tend to overestimate the surface air temperature particularly for a stable stratified lower troposphere at 00 UTC

Temporal and horizontal mismatching

Past studies which are based on less restricted spatiotemporal collocation schemes (e.g. Wang et al. 2013) show that spatial and temporal mismatching provide a minor contribution to temperature differences between radiosondes and satellite profiles. The impact of horizontal and temporal mismatching is analysed separately.

The time difference between collocated satellite products and radiosonde is different for each individual observation (figure 4.13). As atmospheric temperature can vary rapidly in time, temporal mismatching could influence the accuracy of the satellite observations. Typically, one could expect that a larger temporal mismatch would lead to larger deviations. However, no correlation between temporal mismatches and rmse is found (figure 4.14a). The Pearson-Correlation-Coefficient is approximately 0.14 indicating that the rmse of temperatures and the temporal mismatch are not correlated. Large rmse occur independently from large or small temporal mismatches. Computations of rmse profiles for different bins of time differences (figure 4.14b) underline this key conclusion. On the one hand the profile of rmse is at largest for the largest time difference, particularly up to 100 hPa, but compared to other bins deviations are quite small. Results indicate that temporal mismatching has no major impact on the accuracy of the satellite-based time series which leads to a key conclusion. The availability and daily coverage of AIRS and IASI measurements is sufficient to provide temperature profiles of similar quality in six-hour intervals. Data gaps as well as the time shift to the synoptic standard times can be compensated by time interpolation without significant loss of quality.

Geographical location of radiosonde measurements and matched satellite footprint do not coincide in space for many reasons (section 3). The horizontal mismatch therefore could affect the reliability of satellite products. Figure 4.15a underlines that the rmse does not necessarily increase for larger distances between satellite and radiosondes. Time series of temporal mismatch and rmse are nearly uncorrelated ($PCC = 0.15$). Large and small rmse are observed at all bins of horizontal distances (figure 4.15b). While horizontal mismatches and rmse does not show up a relation according to the full profile rmses, slight differences can be worked out for different atmospheric layers. Especially, in the troposphere (350-900 hPa) figure 4.15b displays larger errors (up to 0.5 K) for larger mismatches.

Results imply that horizontal mismatching is not a major factor for the accuracy of the satellite products. Previous studies in the Antarctic (e.g. Wang et al. 2013) demonstrate that horizontal and temporal mismatching is negligible compared to

errors in the retrieval scheme. Most of these studies applied comparison schemes with less stringent requirements of spatial (>100 km) and temporal (<6 h) matching. As this analysis includes collocated satellite data within a 50 km circle around Neumayer Station, horizontal mismatching is therefore confirmed to be a minor factor.

Impact of cloud cover

It is well-known that IR-based satellite retrievals are strongly influenced by clouds. Cloud contamination limits the accuracy of the retrieved profiles. In order to quantify the impact of cloudiness, the radiosonde observations are classified into five categories of cloudiness.

As a result, temperature differences between radiosonde and satellite products increase with increasing cloud coverage. This effect is most pronounced in troposphere, since clouds predominantly occur in this atmospheric layer (figure 4.16, figure 4.17). On average the troposphere's rmse increases by 0.4 K from clearsky to snowfall profiles, while the bias falls into the negative range by nearly 0.7 K.

On the other hand, variations of rmse (0.19 K) and bias (0.15 K) are very weak in the stratosphere, because there are no clouds which could contaminate IR measurements. It is furthermore remarkable that the rmse for clear sky (0.95 K) profiles is larger than for partly clouded scenes (about 0.83 K) in the stratosphere. The number of clear sky samples is only small compared to the other categories. Since the impact of clouds on the rmse/bias is small in the stratosphere due to absence of clouds, the unrepresentative number of clear sky profiles could explain their large deviations in the stratosphere.

At the surface temperature rmse increases from slightly clouded skies (1.24 K) to snowfall events (1.84 K) by 0.6 K. Clear sky profiles on the contrary, display a large rmse (1.63 K) and the strongest bias of -0.50 K. The large deviations at the surface in cloudless conditions can be explained by a strong variability of surface air temperature due to unhindered radiative cooling over the night and heating of the surface at daytime. These processes depend on the position of the sun (variable in time), wind regimes (variable in space and time) and surface properties (variable in space). The temporal and spatial variability of the air temperature cannot be resolved by the satellites as they provide surface temperature averaged for the entire IFOV. Consequently, this could provide an explanation of the high deviations at the surface in the category "clearsky".

Only the synoptic visual observations at Neumayer Station are used for the cloud categorization. This could be a limiting factor for this analysis, because patterns of cloudiness and precipitation vary spatially and temporally. The times of synoptic observations for instance do not necessarily fit the satellite overpass times. Furthermore, the observed cloudiness at Neumayer Station may not correspond to the actual cloudiness at the matched satellite footprint location. For this reason large uncertainties and deviations of rmse and biases could be explained by misclassified profiles.

Surface-based temperature inversions

The acquisition of properties of temperature inversions poses a particular challenge for AIRS and IASI because of the limited vertical resolution of the sounders.

Previous studies have shown that frequency and intensity of temperature inversions in the Antarctic depend on season and geographical location (e.g. Zhang et al., 2011; Boylan et al., 2016). Boylan et al. (2014, 2016) demonstrates that IASI and AIRS temperature profiles commonly overestimate frequency and underestimate intensity of SBTI in the Antarctic. This can be confirmed by this analysis for longer time periods at Neumayer Station as number of detected SBTIs is clearly overestimated by the satellite products for each synoptic time. The largest agreement in SBTI detection is found at 06 UTC, corresponding to the smallest bias in surface temperature (table 4.1). At the other synoptic standard times, the overestimation of SBTI frequencies is related the strong negative biases (-1.18 K to -1.55 K). An underestimation of surface temperature by the satellites (negative bias) in general forces a stabilization of the lowermost troposphere and thus favours detection of surface inversions. This effect is particularly important at times where the lowermost troposphere is typically indifferent or unstable stratified such as 12 and 18 UTC and is responsible for the overestimated frequencies and intensities. Temperature inversions observed anyway (e.g. at 00 and 06 UTC) are only intensified in their intensity by the negative biases.

The intensity of temperature inversions is predominantly underestimated by the satellite products by approximately 1 K except for 18 UTC. The altitude of the maximum temperature of the inversions is individual for each profile and can vary by several 100 meters. Radiosondes are able to record these variations suitably as their vertical resolution is about 5 m. The vertical resolution of AIRS/IASI (~1 km) and the retrieved products (roughly 0.2-0.3 km in lower troposphere) is

several times coarser. The satellite profiles therefore are not capable to capture the structure of SBTIs properly leading to an underestimation of the temperature maximum. Thus, intensities of temperature inversions are also systematically underestimated. The overestimation of SBTI intensity at 18 UTC is consistent with the large negative bias detected at the surface.

This study reveals the potential of IASI and AIRS derived temperature products in the summer atmosphere and is expected to be representative for the entire coastal Eastern Antarctic. Improvements in these satellite products could greatly lead to better representation of temperatures at the tropopause level, the lowermost troposphere and in the lower stratosphere. Detection and intensity of temperature inversions are bound to an accurate surface temperature product. Improvements in IASI's and AIRS' surface air temperature product would therefore result in a more realistic capture of frequency of occurrence and intensity of SBTI's. Overestimation of tropopause temperature is mainly caused by the limited sounder resolution. However, since the warm bias is a continuous and systematic issue, adjustments in the retrieval algorithm could improve the representation of the tropopause in the polar summer atmosphere. In the stratosphere between 50-250 hPa the improvements of the AIRS-only retrieval in particular could reduce the systematic biases at these levels and would lead to a corrected representation of the polar lower stratosphere.

6. Summary and outlook

Embedded in the YOPP-SOP-SH campaign, during the austral summer season 18/19, I conducted in total 339 radiosonde measurements in six hour intervals at the German research station Neumayer III. The resulting temperature data is compared with reconstructed temperature profiles of derived products from IASI and AIRS.

The accuracy of the satellite time series fits the requirements of NWP and the strived measuring precision of the satellite instruments, which is about 1 K in 1 km layers (Aumann et al., 2003; Blumstein et al., 2004). Overall, the resulting rmse is 0.97 K for the entire profiles and is slightly larger in the troposphere (1.06 K) than in the stratosphere (0.90 K). At the surface level the rmse increases up to 1.90 K at surface. The total bias (-0.14 K) shows a similar distribution of deviations and is negative for the troposphere, stratosphere and surface. At the surface large variations of bias are found ranging between -8 and 8 K. Systematic errors occur in particular layers of the atmosphere, for instance at the tropopause level and in the lower stratosphere. The temperature of the tropopause is strongly overestimated, especially in the summer atmosphere regime by more than 0.5 K which is a consequence of the restricted vertical resolution of the sounders. Positive and negative biases between -1 to 1 K appear in the 50-250 hPa layer and are mainly induced by inaccuracies of the AIRS temperature profile in the stratosphere. Diurnal variations of deviations are weak in the troposphere (rmse of 0.15 K) and hardly present in the stratosphere (0.08 K). At the surface rmse and bias show strong fluctuations which is related to the cycle of formation and regeneration of temperature inversions.

No significant correlation is found between rmse and spatial and temporal mismatching. This implies that both, the implemented scheme of spatial collocation (50 km radius) as well as the temporal interpolation of the matched temperature profiles guarantee the coverage of satellite information of similar quality throughout the day. The data post-processing scheme therefore is

suitable for coastal polar locations, where the number of available polar-orbiting satellites is large and surface terrain is predominantly flat, for instance on ice-shelves.

The influence of clouds on the accuracy of the satellite time series is different for each atmospheric layer. In the troposphere, rmse from slightly cloudy or cloudless profiles to heavily cloudy situations increase by roughly 0.4 K, meanwhile the bias decreases by nearly 0.7 K. At the surface the impact of cloudiness is larger. Results reveal that the rmse difference between slightly clouded situations and snowfall events is about 0.6 K. The bias varies from positive (0.33 K, low cloud cover) to negative values (-0.37 K, snowfall). Strikingly high deviations are recorded in clear sky situations showing a strong bias (-0.50 K) and an rmse (1.63 K) of comparable magnitude to that of heavily overcast profiles. These exceptionally large variations can be explained by high variability of surface air temperature. In the stratosphere, the impact of cloudiness is only weak. Conclusively, cloudiness affects the accuracy of the satellite time series, particularly in the troposphere in which clouds predominantly occur.

Corresponding to findings of previous studies (e.g. Boylan et al., 2016), results clearly point out that the frequency of surface-based temperature inversions is overestimated, whereas the intensity is mainly underestimated. The overestimation of frequency can be explained by a strong cool bias at the surface level pretending a stability of the lower troposphere. However, particularly at 12 and 18 UTC the radiosonde profiles measure a neutral or unstable stratification of this layer. Therefore, the negative bias is responsible for the fact that the frequency of inversions detected by satellites around 12 and 18 UTC is twice as high as compared to the radiosondes observations. Intensities of SBTIs are underestimated at all times by approximately 1 K, except for 18 UTC. Temperature inversions are meteorological structures of small vertical extension. The vertical grid of the satellite product is much coarser than the vertical resolution of the radiosonde measurements, therefore position and characteristics of the SBTI's temperature maximum cannot be captured adequately by the satellites. The systematic underestimation of SBTI is consequently caused by the limited satellite resolution capability.

The present thesis provides an assessment of the satellite-derived temperature profiles over the entire polar summer season in a diurnal context at a polar location. Systematic issues are quantified for different atmospheric layers and with respect to key error sources, such as spatiotemporal mismatching and cloudiness. This assessment is only representative for the polar summer season. Results indicate that distribution of errors between satellite and radiosonde

profiles are fundamentally different in the winter atmosphere. Since the winter atmosphere at Neumayer Stations is predominant for large parts of the year, future research should also include observations from this season.

This study shows that clouds have a negative influence on the accuracy of the used IR-based satellite products. As microwave-based measurements are less sensitive to non-precipitating clouds, retrieved products of combined infrared and microwave measurements could be additionally assimilated to improve the reliability and availability of satellite data in clouded situations.

Nowadays, not only temperature profiles are derived from space-borne radiance measurements but also humidity and wind profiles (Aeolus satellite). Future research could extend this analysis on these parameters to provide a complete evaluation of meteorological variables recorded by satellite measurements in the Antarctic.

Our scheme of data processing and spatial collocation of satellite and radiosonde can be applied for any region within the Polar Circle. As part of the YOPP campaign, radiosonde measurements were conducted for various locations of the Arctic and Antarctic providing a unique data set of highly-frequent upper air measurements to be compared on large scales. This gives the unique opportunity to quantify the performance of satellite products for different locations such as continental or mountainous sites and to assess the impact of the YOPP campaign and satellites products on NWP at Polar regions in general.

Bibliography

AIRS (2017a), *AIRS/AMSU/HSB Version 6 Level 2 Product User Guide*, v.1.7.2, edited by E.T. Olsen et al.

AIRS (2017b), *AIRS/AMSU/HSB Version 6 Level 2 Product Levels, Layers and Trapezoids*, v.1.0.2, edited by E.T. Olsen et al.

AIRS Science Team/Joao Teixeira (2013), *AIRS/Aqua L2 Support Retrieval (AIRS-only) V006*, Greenbelt, MD, USA, Goddard Earth Sciences Data and Information Services Center (GES DISC), Accessed: [30th, January 2019 to 17th, February, 2019], doi:10.5067/Aqua/AIRS/DATA208.

Andersson, E., Pailleux, J., Thépaut, J.-N., Eyre, J.R., McNally, A.P., Kelly, G.A. and P. Courtier (1994), *Use of cloud-cleared radiances in three/four-dimensional variational data assimilation*, Q.J.R. Meteorol. Soc., **120**(517), 627-653, doi:10.1002/qj.49712051707.

Andreas, E.L. (1980), *Estimation of heat and mass fluxes over arctic leads*, Mon. Weather Rev., **108**(12), 2057-2063, doi:10.1175/15200493(1980)108<2057:EOHAMF>2.0.CO;2.

Aumann, H.H., Chahine, M.T., Gautier, C., Goldberg, M.D., Kalnay, E., McMillin, L.M., Revercomb, H., Rosenkranz, P.W., Smith, W.L., Staelin, D.H., Strow, L.L. and J. Susskind (2003), *AIRS/AMSU/HSB on the Aqua mission: Design, science objectives, data products, and processing systems*, IEEE Trans. Geosci. Remote Sensing, **41**(2), 253–264, doi:10.1109/TGRS.2002.808356.

Blumstein, D., Chalon, G., Carlier, T., Buil, C., Hébert, P., Maciaszek, T., Ponce, G., Phulpin, T., Tournier, B., Simeoni, D., Astruc, P., Clauss, A., Kayal, G., R. Jegou (2004), *IASI instrument: technical overview and measured performances*, Proc. SPIE 5543, *Infrared Spaceborne Remote Sensing XII*, doi:10.1117/12.560907.

Boylan, P., Wang, J., Cohn, S. A., Fetzer, E., Maddy, E.S. and S. Wong (2015), *Validation of AIRS version 6 temperature profiles and surface-based inversions over Antarctica using Concordiasi dropsonde data*, J. Geophys. Res. Atmos., **120**, 992–1007, doi:10.1002/2014JD022551.

Boylan, P., Wang, J., Cohn, S.A., Hultberg, T. and T. August (2016), *Identification and intercomparison of surface-based inversions over Antarctica from IASI, ERA-Interim, and Concordiasi dropsonde data*, J. Geophys. Res. Atmos., **121**, 9089–9104, doi:10.1002/2015JD024724.

Dang, H.V.T., Lambrigtsen, B. and E. Manning (2017), *AIRS/AMSU/HSB version 6 level 2 performance and test report*, version 1.2.1.

Davis, D., J. B Nowak, J.B., Chen, G., Buhr, M., Arimoto, R., Hogan, A., Eisele, F., Mauldin, L., Tanner, D., Shetter, R., Lefer, B. and P. McMurry (2001), *Unexpected high levels of NO observed at South Pole*, Geophys. Res. Lett., **28**(19), 3625–3628, doi:10.1029/2000GL012584.

Divakarla, M.G., Barnet, C.D., Goldberg, M.D., McMillin, L.M., Maddy, E., Wolf, W., Zhou, L. and X. Liu (2006), *Validation of Atmospheric Infrared Sounder temperature and water vapor retrievals with matched radiosonde measurements and forecasts*, J. Geophys. Res., **111**, doi:10.1029/2005JD006116.

ECMWF (2019), *Global observing system experiments in the ECMWF assimilation system*, Technical Memorandum 839, Research department, edited by Bormann, N., Lawrence, H. and J. Farnan, available at: <https://www.ecmwf.int/en/elibrary>.

EUMETSAT (2017a), *IASI Level 2: Product Generation Specification*, v8E e-signed, Doc. Nr. EPS.SYS.SPE.990013 © EUMETSAT.

EUMETSAT (2017b), *IASI Level 2: Product Guide*, v3E e-signed, Doc. Nr. EUM/OPS-EPS/MAN/04/0033 © EUMETSAT.

EUMETSAT (2018), *IASI L2 PPF v.64 validation Report*, v1-e-signed, Doc. Nr. EUM/RSP/REP/18/974859, © EUMETSAT.

EUMETSAT (2019), *IASI Atmospheric Temperature Water Vapour and Surface Skin Temperature – Metop*, © EUMETSAT [2019].

Feltz, M.L., Borg, L., Knuteson, R.O., Tobin, D., Revercomb, H. and A. Gambacorta (2017), *Assessment of NOAA NUCAPS upper air temperature profiles using COSMIC GPS radio occultation and ARM radiosondes*, J. Geophys. Res. Atmos., **122**, 9130–9153, doi:10.1002/2017JD026504.

Goldberg, M.D., Q, Y., McMillin, L.M., Wolf, W., Zhou, L. and M. Divakarla (2003), *AIRS near-real-time products and algorithms in support of operational numerical weather prediction*, IEEE Trans. Geosci. Remote Sensing, **41**(2), 379–389, doi:10.1109/TGRS.2002.808307.

Hébert, P., Blumstein, D., Buil, C., Carlier, T., Chalon, G., Astruc, P., Clauss, A., Siméoni, D. and B. Tournier (2017), *IASI instrument: technical description and measured performances*, Proc. SPIE 10568, International Conference on Space Optics - ICSO 2004, 1056806, doi:10.1117/12.2308007.

Hultberg, T., and T. August (2013), *The piece-wise linear regression retrieval of temperature, humidity and ozone within the EUMETSAT IASI L2 PPF version 6 paper*, presented in 2013, EUMETSAT Meteorological Satellite Conference Proceedings, EUMETSAT, Vienna, Austria.

Intergovernmental Panel on Climate Change (2013), *Climate Change 2013: The Physical Science Basis. Contribution of Working Group I to the Fifth Assessment Report of the Intergovernmental Panel on Climate Change*, edited by T. F. Stocker et al., 1535, Cambridge Univ. Press, Cambridge, U. K., and New York, doi:10.1017/CBO9781107415324.

Johanson, C.M. and Q. Fu (2007), *Antarctic atmospheric temperature trend patterns from satellite observations*, Geophys. Res. Lett., **34**, L12703, doi:10.1029/2006GL029108.

Kidder, S.Q. and T.H. Vonder Haar (1995a), *Radiative Transfer*, 52-79, in textbook: *Satellite Meteorology: An Introduction*, Academic Press, San Diego, ISBN:0-12-406430-2.

Kidder, S.Q. and T.H. Vonder Haar (1995b), *Temperature and Trace Gases*, 183-196, in textbook: *Satellite Meteorology: An Introduction*, Academic Press, San Diego, ISBN:0-12-406430-2.

Köpke, P. and M. Sachweh (2012a), *Licht und andere elektromagnetische Strahlung*, 57-68, in textbook: *Satellitenmeteorologie*, Verlag Eugen Ulmer Stuttgart, Freiburg, ISBN:978-3-8252-3525-3.

Köpke, P. and M. Sachweh (2012b), *Was passiert mit der Strahlung bis zum Signal am Satelliten?*, 73-98, in textbook: *Satellitenmeteorologie*, Verlag Eugen Ulmer Stuttgart, Freiburg, ISBN:978-3-8252-3525-3.

König-Langlo, G. and B. Loose (2007), *The Meteorological Observatory at Neumayer Stations (GvN and NM-II) Antarctica*, *Polarforschung* 2006, **76** (1), 25-38.

Kottmeier, C., Frey, K. Hasel, M. and O. Eisen (2003), *Sea ice growth in the eastern Weddel Sea in winter*, *J. Geophys. Res.*, **108**(C4), 3125, doi:10.1029/2001JC001087.

Liu, Y. and J.R. Key (2003), *Detection and Analysis of Clear-Sky, Low-Level Atmospheric Temperature Inversions with MODIS*, *J. Atmos. Oceanic Technol.*, **20**, 1727–1737, doi:10.1175/1520-0426(2003)020<1727:DAAOCL>2.0.CO;2.

Mernild, S.H. and G.E. Liston (2010), *The Influence of Air Temperature Inversions on Snowmelt and Glacier Mass Balance Simulations, Ammassalik Island, Souteast Greenland*, *J Appl. Meteor. Climatol.*, **49**, 47–67, do:10.1175/2009JAMC2065.1.

Milstein, A.B., and W.J. Blackwell (2016), *Neural network temperature and moisture retrieval algorithm validation for AIRS/AMSU and CrIS/ATMS*, *J. Geophys. Res. Atmos.*, **121**, 1414–1430, doi:10.1002/2015JD024008.

NASA (2006), *Earth Science Reference Handbook: A guide to NASA's Earth Science Program and Earth Observing Satellite Mission*, edited by Parkinson C.L., Ward, A. and M.D. King.

Polar View (2019), *Polar View ApS*, polarview.aq, 2019-10-15, requested at <https://www.polarview.aq>.

Pougatchev, N., August, T., Calbet, X., Oduleye, O., Schlüssel, P., Stiller, B., Germain, K.St. and G. Bingham (2009), *IASI temperature and water vapor retrievals - error assessment and validation*, *Atmos. Chem. Phys.*, **9**, 6453-6458, doi:10.5194/acp-9-6453-2009.

Parkinson, C.L. (2003), *Aqua: An Earth-Observing Satellite Mission to Examine Water and Other Climate Variables*, *IEEE Trans. Geosci. Remote Sensing*, **41**(2), 173-183, doi:10.1109/TGRS.2002.808319.

Reale, T., Sun, B., Tilley, F.H. and M. Pettey (2012), *The NOAA Products Validation System (NPROVS)*, J. Atmos. Oceanic Technol., **29**, doi:10.1175/JTECH-D-11-00072.1.

Schmithüsen, H. and M. Koch (2019): *Radiosonde measurements from Neumayer Station (2019-02)*. Alfred Wegener Institute, Helmholtz Centre for Polar and Marine Research, Bremerhaven, PANGAEA, doi: Pending.

Schmithüsen, H. and H. Müller (2019a): *Radiosonde measurements from Neumayer Station (2018-11)*. Alfred Wegener Institute, Helmholtz Centre for Polar and Marine Research, Bremerhaven, PANGAEA, doi:10.1594/PANGAEA.900641.

Schmithüsen, H. and H. Müller (2019b): *Radiosonde measurements from Neumayer Station (2018-12)*. Alfred Wegener Institute, Helmholtz Centre for Polar and Marine Research, Bremerhaven, PANGAEA, doi:10.1594/PANGAEA.900642.

Schmithüsen, H. and H. Müller (2019c): *Radiosonde measurements from Neumayer Station (2019-01)*. Alfred Wegener Institute, Helmholtz Centre for Polar and Marine Research, Bremerhaven, PANGAEA, doi:10.1594/PANGAEA.900631.

Scientific Committee on Antarctic Research (2009), *Antarctic Climate Change and the Environment*, edited by Turner, J. et al., SCAR, Cambridge.

Schlüssel, P., Hultberg, T.H., Phillips, P.L., August, T. and X. Calbet (2005), *The operational IASI Level 2 processor*, *Advances in space research*, **36**(5), 982-988, doi:10.1016/j.asr.2005.03.008.

Susskind, J., Barnett, C.D. and J.M. Blaisdell (2003), *Retrieval of Atmospheric and Surface Parameters From AIRS/AMSU/HSB Data in the Presence of Clouds*, IEEE Trans. Geosci. Remote Sensing, **41**(2), 390-409, doi:10.1109/TGRS.2002.808236.

Tao, Z., Blackwall, W.J. and D.H. Staelin (2013), *Error Variance Estimation for Individual Geophysical Parameter Retrievals*, IEEE Trans. Geosci. Remote Sensing, **51**(3), 1718–1227, doi:10.1109/TGRS.2012.2207728.

Vaisala (2013a), *Vaisala Radiosonde RS41 Measurement Performance*, White Paper. Ref. 8B211356EN-A © Vaisala.

Vaisala (2013b), *GPS-based Measurement of Height and Pressure with Vaisala Radiosonde RS41*, White Paper, Ref.B211316-EN-A© Vaisala.

Vaisala (2018), *Vaisala Radiosonde RS41-SGP – accuracy and reliability*, Datasheet Ref. B211444EN-G © Vaisala.

Wang, J., T. Hock, S. A. Cohn, C. Martin, N. Potts, T. Reale, B. Sun, and F. Tilley (2013), *Unprecedented upper air dropsonde observations over Antarctica from the 2010 Concordiasi experiment: Validation of satellite-retrieved temperature profiles*, *Geophys. Res. Lett.*, **40**(6), 1231–1236, doi:10.1002/grl.50246.

Wilks, D.S. (2006a), *Empirical Distributions and Exploratory Data Analysis*, 50-51, in textbook: *Statistical Methods in the Atmospheric Sciences*, Second Edition, Academic Press, San Diego, ISBN:0-12-751966-1.

Wilks, D.S. (2006b), *Forecast Verification*, 278-289, in textbook: *Statistical Methods in the Atmospheric Sciences*, Second Edition, Academic Press, San Diego, ISBN:0-12-751966-1.

Zhang, Y., Seidel, D. J., Golaz, J.-C., Deser, C. and R.A. Tomas (2011), *Climatological characteristics of Arctic and Antarctic surface-based inversions*, *J. Clim.*, **24**(19), 5167–5186, doi:10.1175/2011jcli4004.1.

Acknowledgement

Mein erster Dank gilt Herrn Prof. Dr. Christoph Kottmeier, dem Institutsleiter des IMK-TRO und erstem Gutachter meiner Masterarbeit. Ich bedanke mich bei Ihnen für die Gelegenheit meine Abschlussarbeit in Kooperation mit dem Alfred-Wegener-Institut am IMK-TRO zu verfassen und für die fachliche Beratung, die mich in vielen Phasen des Projekts enorm vorangebracht hat.

Ebenfalls möchte ich mich bei Herrn Prof. Dr. Jan Cermak bedanken für die Betreuung meiner Masterarbeit als zweiter Gutachter. Vielen Dank für Ihr stetes Interesse am Fortschritt meiner Arbeit, sowie für die Integration in Ihre Arbeitsgruppe „Satellitenklimatologie“ des IMK-ASF, die mir auch über das Fachliche hinaus viel bedeutet hat.

Ein ganz besonderer Dank an Herrn Dr. Holger Schmithüsen, dem wissenschaftlichen Koordinator der meteorologischen Observatorien der Neumayer Station und des Forschungsschiffs „Polarstern“, für die Betreuung der Arbeit seitens des AWI's. Ich bedanke mich für Dein lebhaftes Interesse an meiner Forschung und die Beratung in vielen intensiven Diskussionen, speziell aber für die Möglichkeit im Rahmen meines Projekts an einer dreimonatigen, internationalen Messkampagne in der Antarktis mitwirken zu dürfen.

Ich bedanke mich insbesondere auch beim Alfred-Wegener-Institut Helmholtz Zentrum für Polar- und Meeresforschung für die Finanzierung der Kampagne.

Auch der lebhaften Arbeitsgruppe „Satellitenklimatologie“ des IMK-ASF's möchte ich danken für Eure offenen Ohren, zahlreichen Ratschläge und auch für eine schöne Zeit am Campus Nord.

Die Kampagne „Year of Polar Prediction“ hätte an Neumayer III nicht in dem Umfang stattfinden können, wäre ich nicht bei den Radiosondierungen unterstützt worden. Vielen Dank daher den „ÜWI“-Meteorologen Hanno Müller und Michael Koch, die mir bei den Messungen geholfen haben.

Ich bedanke mich zudem bei Sunke Trace-Kleeberg und meiner Schwester Kimberly Krüger für gewissenhaftes und sorgfältiges Korrekturlesen meiner Masterarbeit.

Ein großer Dank gilt auch meinen Mitbewohnerinnen, Freunden und Kommilitonen für Unterstützung und Ablenkung in schwierigeren Zeiten, sowie für eine wundervolle Zeit in Karlsruhe während des Studiums und natürlich auch darüber hinaus.

Meinen Geschwistern, meinen Eltern, sowie meiner gesamten Familie danke ich für die Unterstützung während meines gesamten Studiums. Ihr wart immer dann für mich da, wenn ich Euch gebraucht habe!

Declaration of authorship

I hereby declare that the thesis submitted is my own unaided work. All direct or indirect sources used are acknowledged as references. I am aware that the thesis in digital form can be examined for the use of unauthorized aid and to determine whether the thesis as a whole or parts incorporated in it may be deemed as plagiarism.

For the comparison of my work with existing sources I agree that it shall be entered in a database where it shall also remain after examination, to enable comparison with future theses submitted. Further rights of reproduction and usage, however, are not granted here. This paper was not previously presented to another examination board and has not been published.

Karlsruhe, 15.11.2019

Konstantin Krüger